INCREASED STRENGTHENING OF AUSTENITIC ALLOYS THROUGH DUAL AGING

Annie Ma
(M. S. thesis)

June 1978

Prepared for the U. S. Department of Energy
under Contract W-7405-ENG-48

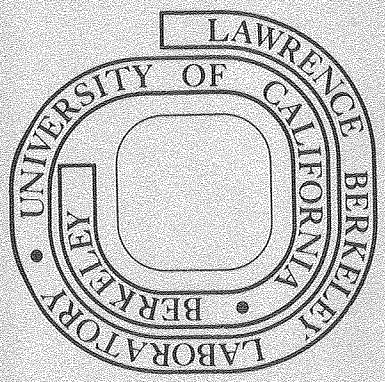

INCREASED STRENGTHENING OF AUSTENITIC ALLOYS THROUGH DUAL AGING

Annie Ma

Inorganic Materials Resarch Division, Lawrence Berkeley Laboratory and Department of Materials Science and Engineering, College of Engineering; University of California, Berkeley, California

ABSTRACT

The research reported herein is a study of the effect of solution treatment, single and duplex isothermal aging heat treatments on an Fe-Ni-Ti-Al austenitic alloy hardened by γ' precipitation. Sequential heat treatments were performed and studied in order to develop a systematic process for achieving very high strength austenite through thermal processing alone.

Room temperature tensile tests were carried out. Alloys receiving double aging treatments were found to achieve mechanical properties superior to those aged at a given temperature. An optimum level of yield strength (172Ksi) along with good elaongation (20%) was obtained from a two-step aging process.

Structural examination indicated that overaging was retarded by secondary aging. The formation and growth of cellular precipitates were suppressed. Resistivity changes were measured on wire specimens to study the early stages of precipitation. Resistivity peaks were observed during secondary aging indicating evidence of secondary precipitation.

TABLE OF CONTENTS

This work was done with support from the U.S. Department Of Energy.

I. INTRODUCTION

Age-hardening through the precipitation of intermetalic compounds, particularly by the addition of Al and/or Ti, has been in commercial use for some time. Most of the earlier work was largely confined to nickel-base alloys [1-5]. But in the last two decades, considerable attention had been given to the strengthening of low-carbon austenitic steels [6-14], such as alloy A-286, because of their potential for high temperature applications.

All the possible phases that can be found in austenitic iron alloys are listed in Table I [15]. Most phases do not serve useful hardening functions and their presence is found to be detrimental to mechanical properties. However one of the B_3A phases is the most commonly used [6-12,15-16] hardening precipitate for austenitic steel, γ' $Ni_3(TiAl)$, a transitional phase. During the early stage of precipitation, γ' has an fcc ($L1_2$) structure (Figure 1a) and forms as spherical particles distributed randomly in the matrix. But in the later stages in the aging process, the equilibrium γ' is replaced by η, a cellular or Widmanstatten type of precipitate involving the cp hexagonal (DO_{24}) phase Ni_3Ti (Figure 1b). The occurence of cellular precipitation is detrimental to mechanical properties since it is preferentially nucleated along grain boundaries, resulting in a decrease in strength and ductility.

The control and minimization of grain boundary precipition, therefore, is a primary goal for achieving a high strength alloy with reasonable residual toughness. Three general approaches have been employed: altering alloy chemistry, cold working and thermal heat treatment. These techniques, applied singly or jointly, affect the precipitation behavior and will be described briefly below.

(A) Alloy Addition

In general, the rate of aging increases with increasing supersaturation. In Fe-Ni austenites, a high Ti content yields a maximum aging response due to the large misfit between the precipitate and the matrix. But the benefit of this increase is offset by a tendency toward rapid overaging. An Al addition [1,11] can suppress the start of the grain boundary reaction, but since Al is a smaller atom than Ti it reduces the coherency strain and increases the time to reach peak hardness. The formation of deleterious sigma phase also occurs at high Al content [9]. An optimum content of Ti + Al in Fe-Ni austenitic steels was found [11] to be at approximately 23 to 1 atomic ratio of Ti to Al, though a slightly lower ratio (11.7) was reported [1] for Ni-based alloys. Grain boundary precipitation is also retarded by other alloy species, for example, boron [1], which does not directly participate in the precipitation process.

(B) Cold Work

Some of the energy expended in cold work appears as strain energy stored in the metal [17] associated with dislocations which are introduced by plastic deformation. Each dislocation is a crystal defect which may serve as a favorable nucleation site during subsequent aging. The application of cold work after solution treatment hence accelerates the aging response and has been found [12] to raise the proof stress substantially. However, cold work is generally unattractive from a practial point of view because of the difficulty of deformation-processing relatively thick sections.

(C) Thermal Treatment

Age-hardening kinetics are determined by the rate of nucleation and growth of the precipitates. Several features [18] are observed in precipitation hardening:

(a) The formation of metastable fine zones precedes that of the equilibrium phase.

(b) The strength of the precipitate-hardened alloy increases with the density of precipitate particles.

(c) The hardness goes through a maximum with aging time.

(d) The maximum hardness is reached sooner at higher temperature.

(e) The ultimate hardness decreases as the aging temperature increases.

The formation and maintenance of a fine precipitate distribution is critical in developing high strengths. A careful consideration of the relevant metallurgical reaction suggests the utilization of a two-step aging process. Since the development of fine γ' particles is determined by the diffusion of solute, a higher aging temperature enhances the rate of homogeneous nucleation. Subsequent aging treatment at a lower temperature can delay the coarsening kinetics and allow the particles to grow slowly. Hence by aging the alloy at a high temperature for a short time followed by a second aging at a lower temperature, both the size and volume fraction of the precipitates can be controlled. Blower and Mayer [12] had successfully applied the double aging treatment to austenitic stainless steels to attain high tensile strengths. However, the relationships between the nature of the precipitation process induced on secondary aging and the resulting changes in strength is not well understood.

This research was undertaken to systematically study the effect of solution heat treatment, single and duplex isothermal aging heat treatment on the aging response and mechanical properties of an Fe-Ni-Ti-Al austenite hardened by γ' precipitation. The secondary aging reaction, in particular, was given more attention to establish a technique for achieving very high strength austenite through

thermal processing alone. The resistivity technique was also used to investigate the kinetics of precipitate formation at the early stage.

II. EXPERIMENTAL PROCEDURE

(A) Material Preparation

The alloy, with nominal composition Fe-36Ni-3Ti-Ø.5Al was made from high purity (99.9%) iron, nickel, titanium and aluminum. A comparison of the nominal and actual composition is given in Table II.

The material was melted in a 11-Kg induction furnace and cast in a copper chill mold. The resulting ingot was then homogenized at 12ØØ^{o}C for 24 hours and furnace cooled in an argon atmosphere. It was then reheated to 11ØØ^{o}C and upset cross-forged into a Ø.5x2 inch square plate and subsequently water quenched. Sections of different dimensions were cut out along the longitudinal direction for testing.

Wire specimens for resistivity studies were prepared by cold rolling a bar sample (cross-section 5/6 inch sq.) to a Ø.2 inch square bar which was further swaged to a Ø.ØØ9-inch diameter rod. Finally the sample was wire drawn through a die which allowed a reduction of 5% per pass to an ultimate diameter of Ø.ØØ25 inch. All the operations were carried out at room temperature. Imperfections were carefully removed with sand paper between passes to produce a high quality wire.

(B) Heat Treatment

Milling and polishing were performed on every specimen before each heat treatment to ensure the complete removal of any oxidation. For specimens requiring isothermal heating, a resistance type chamber furnace was used. Each specimen was sealed in stainless steel bag filled with argon gas. Solution treating was carried out in the range of 850-1150^{o}C, at 50^{o}C intervals. Each heat treatment was followed by water quenching.

A gradient furnace was set up for the purpose of examining hardness as a function of aging temperature. A 20-inch tube furnace, with 1.5-inch inner diameter, was monitored by a furnace controller through the insertion of a thermocouple into the center. Part of the heating element in one end of the furnace was removed to obtain a temperature range of 550^{o}C to 850^{o}C. The furnace was set in an upright position. Bar specimens (6 inch x 0.625 inch square) were drilled and tapped and solution heat treated isothermally. Eight thermocouples were spot welded and secured to each specimen after it had been attached to a specimen holder by a set screw. The specimen was then suspended and lowered into the furnace. The temperature at each thermocouple was recorded automatically every five minutes. The range of temperatures could be varied by either adjusting the furnace temperature or the height of the suspension. The specimen was periodically taken out of the furnace to study the effect of aging time on hardness.

ardness tests were conducted along the specimen corresponding to the different aging temperatures.

(C) Mechanical Testing

(a) Hardness Testing

All specimens to be tested for hardness were carefully polished to remove surface irregularities. A Wilson Rockwell Hardness Tester was used. At least four measurements were made for each data point. The results were presented as an overall average. In all cases, testing was done on the Rockwell C scale, with a diamond Braile indenter and a major load of 150 Kg.

(b) Tensile Testing

All tensile testings were performed on an Instron Testing machine at a cross head speed of 0.05 cm/min at room temperature. A schematic of the subsize tensile specimen is shown in Figure 2. Two specimens were tested for each datum. The yield strengths were reported as the load required at a 0.2% nominal strain offset from the elastic portion of the stress-strain curve.

(D) Microscopy

(a) Optical

All samples were either cold mounted or Baklite mounted using a Struers hot press. They were subsequently

hand polished to 4/Ø grade paper, corresponding to a scatch size of 1Ø microns. Then the scratches were further reduced to ~Ø.25 um using diamond paste on a rotating wheel. Finally they were chemically etched in a H_2O + 4% HF solution for 1Ø seconds. Overetching was to be avoided when a revelation of grain boundary structures was desired.

All micrographs were taken on a Zeiss 64559 metallograph using Polaroid type 55 positive/negative films.

(b) SEM

All fracture surfaces from the tensile tests were examined in a JEOLCO JEM-U3 scanning electron microscope with secondary electron emission at 25KV.

(E) Resistivity Tests

A circuit diagram for the resistivity experiment is shown in Figure 3, the design of which was a modification from Colner and Zmeskal [1]. A 5-inch wire was spotwelded to two stainless steel rods at the ends and insulated platinum wires used as potentials leads were spot welded 2 inches apart on the specimen. The specimen assembly, shown in Figure 4 was then placed in the center of tube furnace where the temperature variation was less than $1^{o}C$ over a range of 2 inches. Argon gas was fed into the furnace at a constant rate. Prior to the start of the experiment, all electronics were turned on and allowed to reach a steady state. Solu-

tion treating at 1100°C was accomplished by electrical resistance heating with AC current. By throwing the swith to the DC position and simultaneouly increasing the argon flow, the specimen was quenched rapidly to the furnace (aging) temperature and a constant DC current was allowed to flow. The difference in voltage across the 2-inch section of the specimen was amplified by a differential amplifier and recorded on a chart. For the dual aging specimens, the first aging was carried out by AC resistance heating.

The resistivity change was expressed as a percentage, $100x(\rho_t-\rho_o)/\rho_o$, where ρ_o is the resistivity immediately after quenching and ρ_t is the resistivity reading at given t.

III. RESULT AND ANALYSES

(A) Kinetics and morphology of precipitation

Typical curves of hardness vs single aging time for alloys aged at 660-780°C are shown in Figure 5. The results demonstrate that substantial increase in hardness occurs. As indicated by the occurence of hardness peaks, the kinetics of precipitation is faster at higher temperatures. This is due to the increased growth rate, since growth is a diffusion-controlled process, enabling the particles to grow rapidly. Consequently overaging was also accelerated giving a decrease in the observed hardness at longer time. If a lower aging temperature was used, the solid solution was more supersatuated with solute. Hence the intensity of precipitation is higher giving rise to a higher ultimate hardness. A picture of γ' precipitates from a similar class of alloys (Fe-Ni-Ti-Mo) is shown in Figure 6.

When the maximum hardness is reached, cellular precipitates begin to form. Precpitates of this type invariably nucleate along the grain boundaries in colonies, as shown in Figures 7a and 7b. They consist of lamallae or rod shaped Ni_3Ti particles protruding into the matrix. TEM studies [11] showed that this phase continuously loses coherency with the austenitic matrix as overaging proceeds. Clark and Pickering [10] had reported the observation of zones denuded of γ' at the cellular interface suggesting that γ'

was providing the solute for the growth of the cellular Ni_3Ti.

(B) Sequential study of aging reaction

(a) Effect of solution treatment temperature

Specimens tested were given different solution treatments, quenched and then aged at 740°C for 4 hours. The resulting tensile properties are shown in Figure 8. With preaging solution treatment temperatures in the range of 850-1150°C, maxima appear in the tensile and yield strength and %RA curves at around the solution treatment temperature of 900°C. The % El, however, drops when the alloy is solution treated at 1100°C or higher. Treatment temperature variation within the range tested had little effect on the hardness. This observation was also reported by Blower and Mayer [12].

The poor ductility resulting from solution heat treating at high temperature is readily explained after an examination of the fracture surfaces (Figure 9). Specimens solution treated at 1100°C failed by intergranular fracture. Large cleaved facets are visible along with cracks at the grain boundaries. However, the optical micrograph of the same specimen (Figure 11.a) shows very little grain boundary precipitation, the appearance of which was usually responsible for the observed failure mode. The mechanisms

that cause this mode of failure have not been determined.

Figure 9b is a scannig electron micrograph of a "cup and cone" fracture surface. The predominantly dimpled transgranular fracture mode for the 950°C solution treatment is in good agreement with the peak elongation and reduction in area data. The microstructure (Figure 11b) also reveals very "clean" grain boundaries. Solution treating at still lower temperatures again leads to an intergranular fracture mode. Figure 11c shows that a considerable amount of overaging had taken place. This was suspected to be the result of the low solution treating temperature, close to the precipitate solvus temperature. Although microstructural studies of the as solution treated and quenched structures did not show any grain boundary precipitation at temperatures below 900°C, it is possible that precipitates were not completely dissolved during solutioning process. Overaging subsequently took place during the aging heat treatment. The cleavages on the fracture surface however, are much finer since the grain size decreases with decreasing solution treatment temperatures. A measure of grain size vs solution heat treatment temperature is shown in Figure 10.

From the above results, it is clear that the optimum solution heat treating temperature lies in the range 950-1000°C. The 950°C solution temperature was adopted for

the majority of the subsequent heat treatments. Pictures of the as solution treated and quenched structure at 950°C are shown in Figure 12.

(b) Effect of primary aging

The mechanical properties following aging at 670°C and 745°C are shown in Figure 13 and 14. An incubation period is observed at the early stage of aging at low temperature. The maximum yield strength was not reached until after 70 hours at 670°C, as compared to 4 hours at 745°C. The value of % elongation decreases continuously with aging time. Both the ultimate tensile and yield strength at 670°C are higher than those obtained at 745°C, in qualitative agreement with the hardness result as indicated in Fig. 5.

The strengthening mechanism [1,10,11,15] is generally believed to be the γ' precipitation. A large volume fraction of fine precipitates with small inter-particle distance is characteristic of an optimum precipitation strengthened alloy. As deformation proceeds, the movement of dislocations is hindered by the fine distribution of γ' particles.

The microstructures of the aged alloys shown in Figures 15 and 16 show clearly that even though the precipitation kinetics differ, the general morphology of the pre-

cipitates obtained is quite similar. The Widmanstatten form of precipitation was not observed in this study, probably due to the low aging temperatures used.

(c) Effect of double aging

To study the effects of secondary aging, a second aging treatment was applied to alloys previous aged at a given temperature. The first aging time was chosen such that the alloys were either in (i) an underaged or (ii) a fully aged condition prior to the second aging. A comparison of the resulting mechanical properties (Figures 17 and 18) reveals two characteristics:

(1) The specimen that was in the fully aged condition attains a higher strength after reaging than one that was underaged and subsequently reaged .

(2) The ultimate strength of the reaged specimens is higher than one that is aged once at either temperatures.

The factors that contribute to the increase in strength are not entirely clear. It is possible that reaging at a lower temperature promotes further precipitation. Since the driving force for homogeneous nucleation is higher when the matrix becomes more supersaturated. An independent precipitation may have taken place. Another possibility is that vacancies or solute-rich zones form during quenching down from the first aging temperature. These

zones may serve as nucleation sites during subsequent aging. This would also induce a secondary precipitation. It is also possible that no further precipitation has actually taken place and the resulting increase in strength is due to other metallurgical variables. The validity of these assumptions, however, needs to be proven.

Comparison of Figure 19 with either Figure 15 or 16 shows that the amount of cellular precipitates is less in the double aged specimen than that in one aged at constant temperature for the same period of time, even though the double-aged specimen has achieved higher hardness. A lower reaging temperature appears to retard the growth of cellular precipitation. Since the solute must precipitate out of the supersaturated solid solution, it provides indirect evidence that the formation of "new" γ' has occured. Additional precipitation may have taken place in the second aging process.

(C) Correlation of precipitation with electrical resistivity

To study the early stage of secondary precipitation, the presence of the secondary precipitates has to be determined. During the secondary aging, the abundance of solute is considerably lower than the first aging process. These secondary precipitates, if present, must be very small and very coherent. Jin and Hwang [24] applied

transmission electron microscopy to study this phenomenum but failed to detect any direct contrast effect of any precipitates, nor did they observe any scattering or streaks in the diffraction pattern. The resolution of this precipitate may require very sophisticated microscopy. It was therefore decided that the use of resistivity techniques was the most promising approach to investigating the secondary aging process. Electrical resistivity has frequently been used to study the progress of precipitation phenomena. It is experimentally [14,19-23] shown that the resistivity generally rises and drops as the decomposition of a supersaturated solution proceeds. The question of the origin of this anomalous increase is not fully resolved. Herman [21] and Panseri [22], in a study of precipitation in Al-Zn alloys, were able to use small angle X-ray scattering to measure the size of zones during the very early stage of precipitation. A zone radius of approximately 9A^{o} was found to be associated with the resistance maximum observed during aging. It is now generally accepted that when the size of a zones reaches a critical diameter equal to the wavelength of the conducting electrons, maximum scattering of electrons occurs corresponding to an increase in electrical resistance. As growth continues, the coalescence of zones into larger particles reduces the number of scattering centers, causing a decrease in resistance.

The effect of aging time on the resistivity change

at 670°C is plotted in Figure 20. The shape of the curve is in good agreement with previous results [14] on 4%Ti stainless steel. An incubation period is observed indicating the slow formation of zones at low temperature. The maximum resistivity of a specimen tested at 745°C occured too rapidly to be recorded. The time duration was probably in the order of seconds.

Similar experiments were performed on specimens aged at 745° prior to the resistivity measurements and the results are shown in Figure 21. Clearly, the time to reach maximum resistivity decreases with increasing second aging temperature. first aging treatment.

The broadness of the peaks gives additional evidence that the intensity of precipitation is higher at lower temperatures. The ultimate resistivity values indicate that the intensity of zone formation is higher when the temperature difference between the two aging temperatures increases. Upon reaging at higher temperatures (700 and 800°C), the resistivity was found to go up after the appearance of an initial peak. An examination of the microstructure was not able to reveal any difference in the as aged condition.It is suspected that the increase is caused by oxidation which becomes increasingly significant at high temperatures.

A measurement of the hardness, shown in Figure 22,

indicates that hardening results from the second aging in all cases. A small decrease in the second aging temperature was sufficient to initiate additional precipitation. The data also suggest that overaging is delayed by an amount of time proportional to the temperature difference. A picture of the reaged structure at 700°C for 10 hours is shown in Figure 23.

The possible source of error in the resistivity experiment was in the accuracy with which the data were taken. The inaccuracy of the instruments was compensated since only the difference of resistivity was measured. Moreover, all the electronics were allowed to approach steady state before any measurements were taken. One possible factor that may lead to erroneous result is the oxidation in the specimen (in spite of the argon enviroment) causing higher resistivity readings. This may be the dominant factor causing the monotonic increase in resistivity after the initial peak (Figure 21) as discussed before. Another factor that may affect the results is the rate of quenching down the specimens. Since this process is highly temperature-dependent, a difference in the quenching rate may produce metallurgical variation, for example, the defect density, which may result in different resistivity. Defects may also have been introduced from the cold wire drawing process or in the handling of the specimen during assembly. However, the data was found to be reproducible especially at low

temperature. Therefore it was believed that the results are at least qualitatively valid in indicating the secondary precipitation process.

IV. CONCLUSION

(1) Precipitation in the Fe-Ni-Ti-Al system results in the formation of γ' particles which upon overaging, assume a cellular structure along the grain boundaries. No Widmanstatten precipitation was observed.

(2) An optimum range of solution heat treating temperature was found to be 950-1000^{o}C. Alloys solution heat treated above 1000^{o}C exibit an intergranular fracture mode. Solution treating at below 950^{o}C accelerates overaging and causes cellular precipitates to form, again promoting intergranular fracture.

(3) Alloys receiving double aging treatment achieve mechanical properties superior to those aged at a given temperature. A higher strength can be obtained in a much shorter period of time.

(4) The second aging treatment appears to retard the formation and growth of cellular precipitation. This process is beneficial to mechanical properties.

(5) Resistivity peaks were observed in all cases of secondary aging, and the data were in good agreement with existing theory. Although it was not conclusively proven in the present study, evidence was obtained suggesting a secondary precipitation process.

ACKNOWLEGEMENTS

Special thanks are due to my research advisor, Professor J. W. Morris Jr., for his unfailing guidance and support throughout the course of this investigation. I am also grateful to Dr. D. Klahn and Mr. K. M. Chang for many stimulating discussions. Finally I would like to thank Mr. G. Ho for his encouragement and emotional support.

This work was supported by the U. S. Energy Research and Development Administration.

REFERENCES

1. J. R. Mihalisin and R. F. Decker, Trans. TMS-AIME, 1960, Vol. 218, p. 507.

2. R. W. Guard and J. H. Westbrook, Trans. TMS-AIME, 1959, Vol. 215, p. 807.

3. A. V. Dean and R. C. Owen, J. Inst. of Metals, 1962, Vol. 100, p. 181.

4. R. Cozar and A. Pinean, Met. Trans., 1973, Vol. 4, p. 47.

5. C. Ravindran and M. C. Chaturvedi, Met. Trans., Vol. 6A, 1975, p. 213.

6. P. D. Parsons and J. Nutting, J. Iron Steel Inst., 1969, Vol. 20T, p. 230.

7. F. G. Wilson and F. B. Pickering, J. Iron Steel Inst., 1969, Vol. 207, p. 490.

8. J. K. Abraham, J. K. Jackson and L. Leonard, Trans. ASM. 1968, Vol. 61, p. 239.

9. H. J. Beattie Jr. and W. C. Hagel, JOM, July 1957, p. 911.

10. B. R. Clark and F. B. Pickering, J. Iron Steel Inst., 1967, Vol. 205, p. 70.

11. F. G. Wilson and F. B. Pickering, J. Iron Steel Inst., 1966, Vol. 204, p. 628.

12. R. Blower and G. Mayer, J. Iron Steel Inst., 1963, Vol, 201, p. 933.

13. R. G. Yeo, Trans. TMS-AIME, 1963, Vol. 227, p. 884.

14. F. G. wilson and F. B. Pickering, Acta Met., 1968, Vol. 16, p. 115.

15. R. F. Decker and S. Floreen, "Precipitation from Irom-Based Alloys," G. R. Speich and J. B. Clark ed., AIME, 1965, p. 69.

16. B. Cozar and A. Pineau, Met. Trans., 1974, Vol. 5, p. 2571.

17. R. E. Reed-Hill, "Physical Metallurgy Principles," (D. Van Nostrand Co. Inc.), N. J. 1964, p. 175.

18. P. G. Shewmon, "Transformation in Metals," (McGraw-Hill, New York, 1969), p. 286.

19. W. H. Colner and O. Zmeskal, Trans. Am. Soc. Metals, 1952, Vol. 44, p. 1158.

20. W. A. Harrison, Acta Met, March 1960, Vol. 8, p. 168.

21. H. Herman, J. B. Cohen and M. E. Fine, Acta Met, January 1963, Vol. 11, p. 43.

22. C. Panseri and T. Federighi, Acta Met, 1960, Vol. 8, p. 217.

23. A. J. Hillel, J. T. Edwards and P. Wilkes, Phil. Mag., 1972, Vol. 32, p. 189.

24. S. Jin and D. Hwang, Met Trans, 1976, Vol. 7A, p. 745.

Table I

OCCURENCE OF PHASES IN BINARY AND TERNARY TRANSITION ELEMENT SYSTEMS

B Transition Element	A Element: Group IV (4e/a)			Group V (5e/a)			Group VI (6e/a)			BB'
	Ti	Zr	Hf	V	Nb	Ta	Cr	Mo	W	
Mn (7e/a)	B_2A Chi Sigma	B_2A Chi	B_2A Chi	BA Chi Sigma	B_2A Chi	B_2A Chi	Chi Sigma	Chi Sigma	Chi	
Fe (8e/a)	B_2A BA Chi	B_2A	B_2A	BA Chi Sigma	B_2A Sigma	B_2A Sigma	Sigma	B_2A Mu Chi Sigma	B_2A Mu	FeAl FeCo
Co (9e/a)	B_2A BA G	B_2A BA G	B_2A BA G	B_3A Chi Sigma	B_2A G	B_2A G	Sigma	B_3A Mu Sigma	B_3A Mu	CoAl
Ni (10e/a)	B_3A BA G	G	G	B_3A Chi Sigma G	B_3A Mu G	B_3A Mu G	Sigma	B_3A		Beta (NiAl)

TABLE II

Chemical Composition

Ingot No.	Designation	Composition (wt%)				
		Ni	Ti	Al	C	Fe
762-7	Fe-36Ni-3Ti-0.5Al	36.6	2.89	0.43	<0.001	Bal

PICTURE CAPTIONS

1. Atomic arrangement in the unit cell of (a) (Ll_2) γ' b(DO_{24}) Ni_3Ti

2. Diagram of round tensile specimen

3. Circuit diagram for resistivity measurement

4. Specimen assembly in resistivity measurement

5. The effect of aging time on hardness in the temperature range 660-780°C

6. TEM picture of γ' in Fe-32Ni-3Ti-0.5Al-1Mo-0.3V-0.01B

7. Optical micrographs of alloy overaged at 745°C for 7 hours x1570

8. Effect of solution heat treating temperature on the strength and elongation after aging at 740°C for 4 hrs

9. SEM micrographs of fracture surfaces for specimens solution heat treated at (a) 1100°C, (b) 950°C and (c) 850°C

10. Effect of solution heat treating temperature on grain size

11 Micrographs of the as aged structure previously solution heat treated at (a) 1100,°C, x100 (b) 950°C, x470, (c) 850°C, x470.

12. (a) Microgaph of alloy solution heat treated at 950°C x125
(b) SEM micrograph of fracture surface solution heat treated at 950°C x1500

13. Effect of aging time on the strength and elongation of alloy aged at 670°C

14. Effect of aging time on the strength and elongation of alloy aged at 745°C

15. Micrographs of the alloy aged at 670°C for (a) 2 hrs, (b) 9 hrs, (c) 16 hrs, (d) 64 hrs x400

16. Micrographs of the alloy aged at 745°C for (a) 2 hrs, (b) 4 hrs, (c) 9 hrs, (d) 20 hrs. x400

17. Effect of second aging time on the strength and elongation (670°C) for the alloy previously aged at 745°C for 2 hrs

18. Effect of second aging time on the strength and elongation (at 670°C) for the alloy previously aged at 745°C for 6 hrs

19. Micrographs of the alloy aged at 745°C for 6 hrs and at 670°C for (a) 4 hrs, (b) 8 hrs, (c) 16 hrs, (d) 32 hrs. x400

20. Plot of resistivity change vs aging time at 670°C

21. Plot of resistivity change vs second aging time. All specimens were aged at 745°C for 2 hrs

22. Plot of hardness vs total aging time

23. Micrographs of wire specimen aged at 745°C for 2 hrs plus 700°C for 10 hrs, x1570

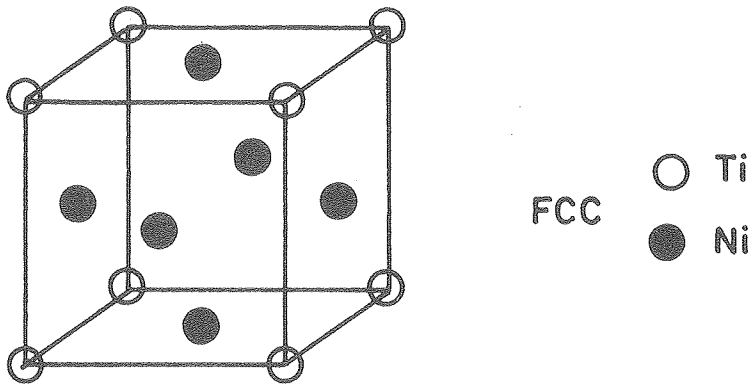

(a)

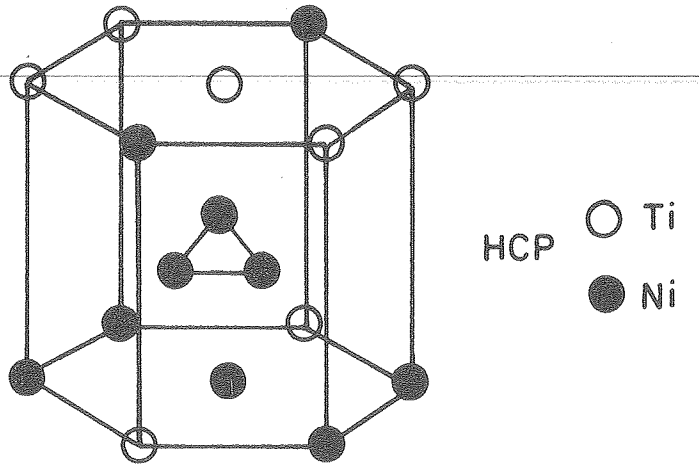

XBL 785-5027

Figure 1

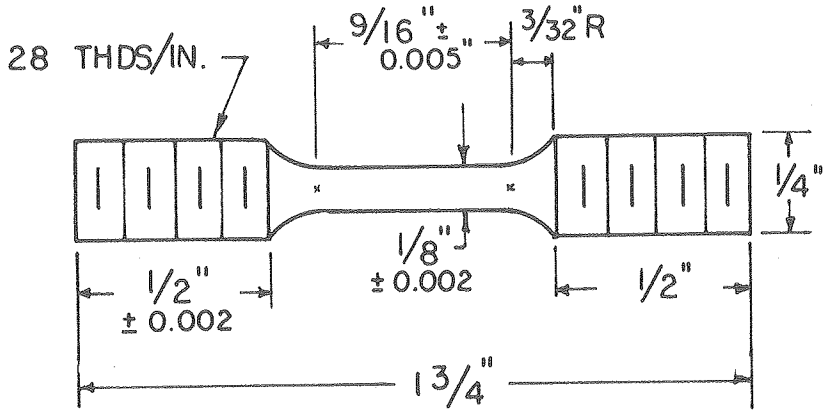

XBL 785-4994

Figure 2

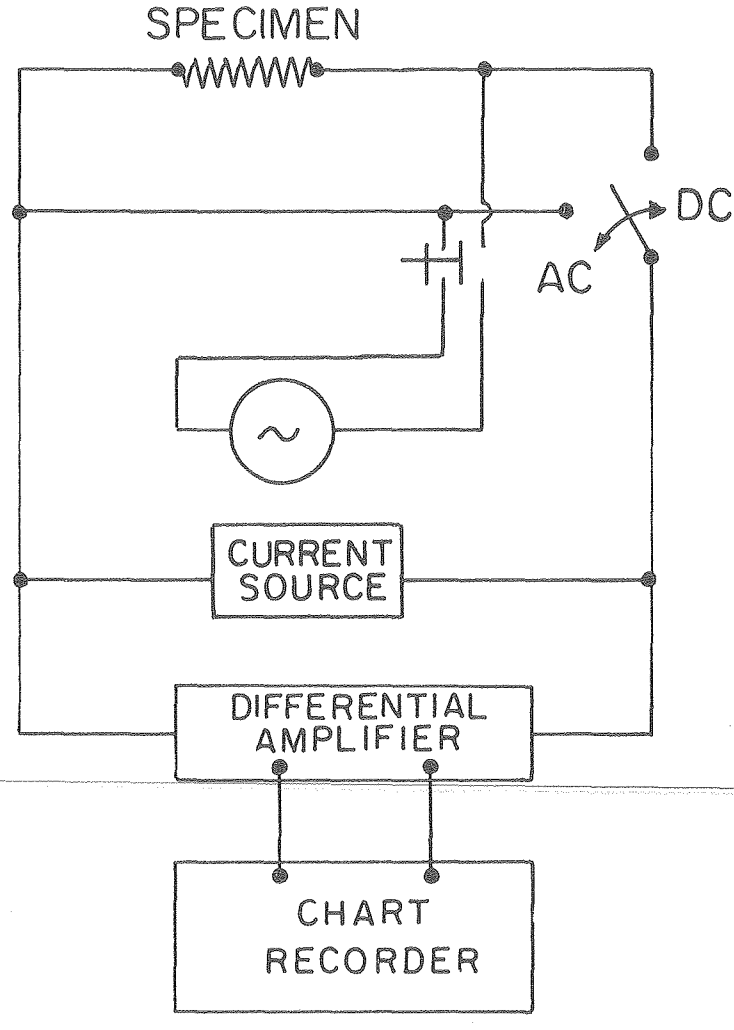

CIRCUIT DIAGRAM

XBL785-4992

Figure 3

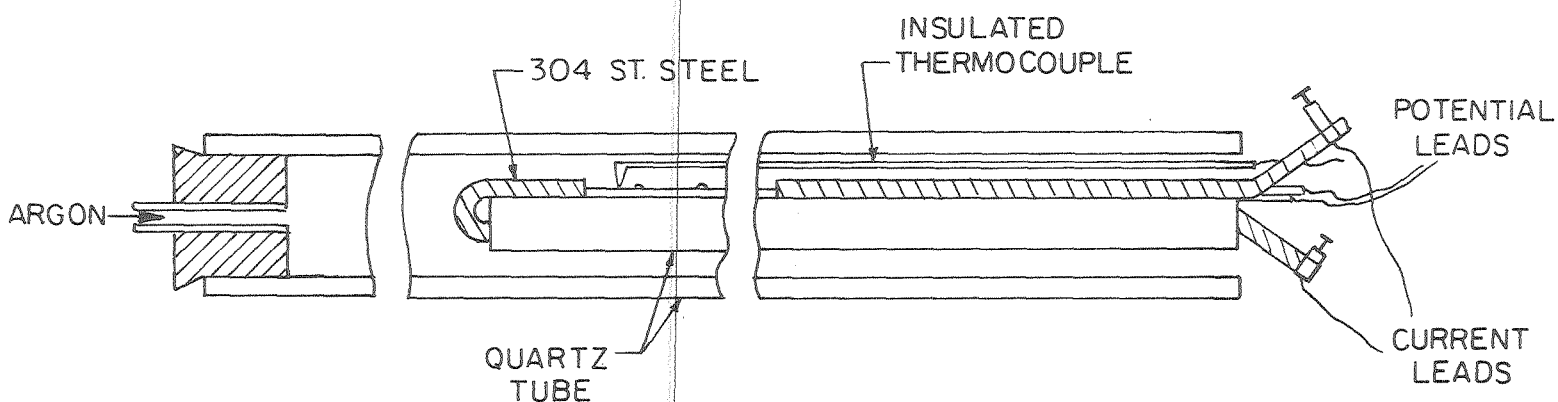

SPECIMEN ASSEMBLY

XBL785-4993

Figure 4

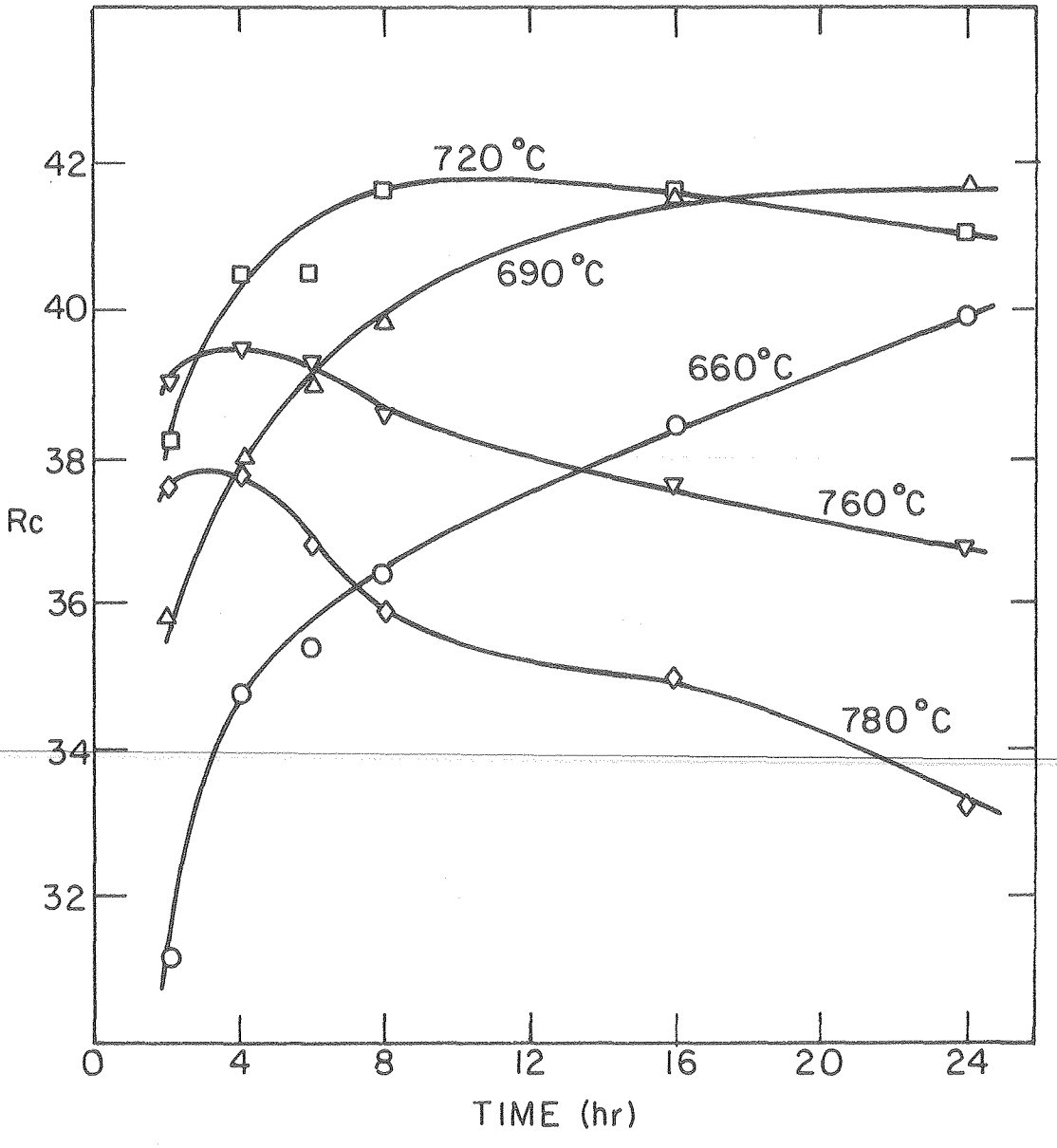
720°C
690°C
660°C
760°C
780°C
42
40
38
36
34
32
Rc
0
4
8
12
16
20
24
TIME (hr)
XBL785-5004

Figure 5

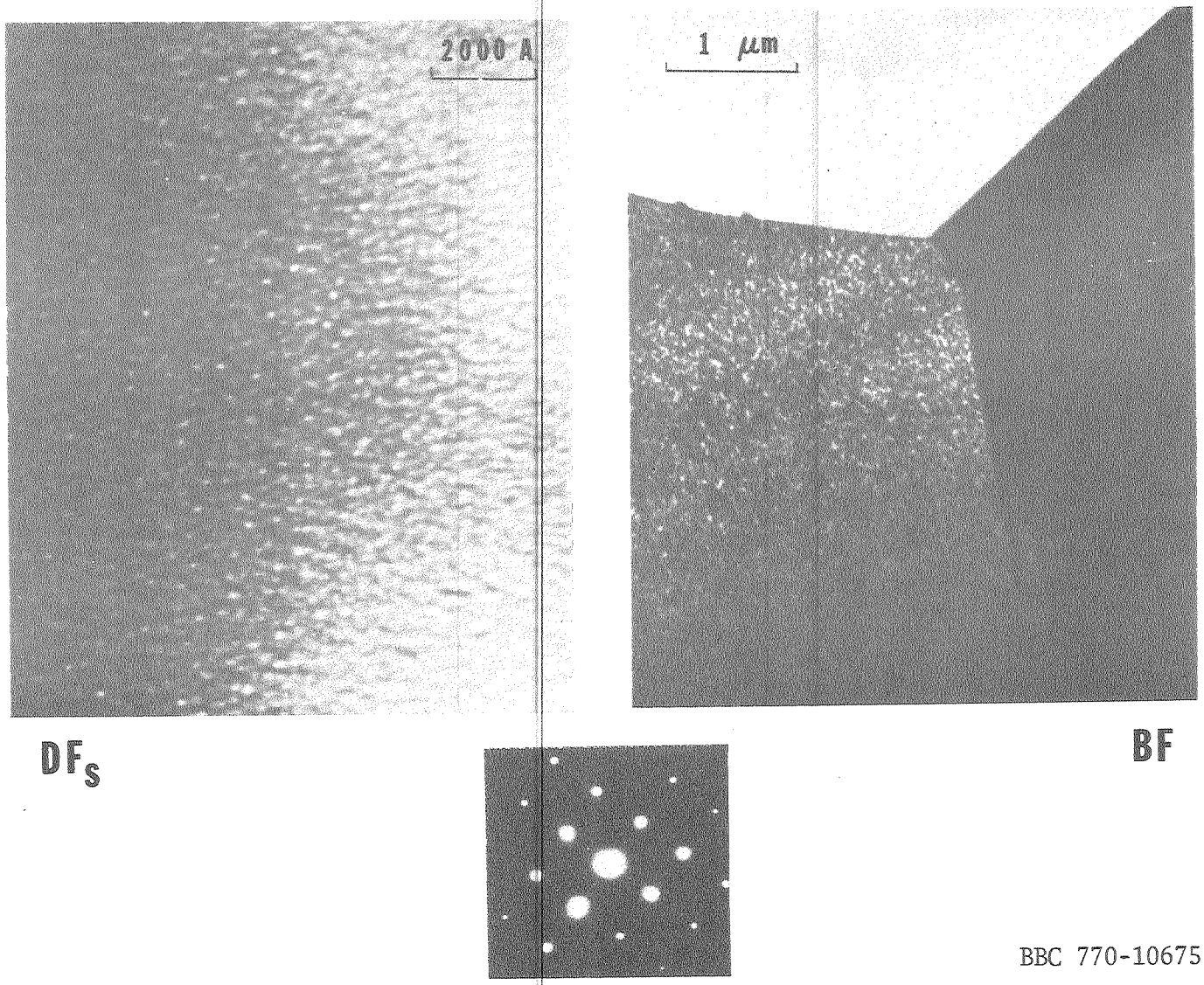

BBC 770-10675

Figure 6

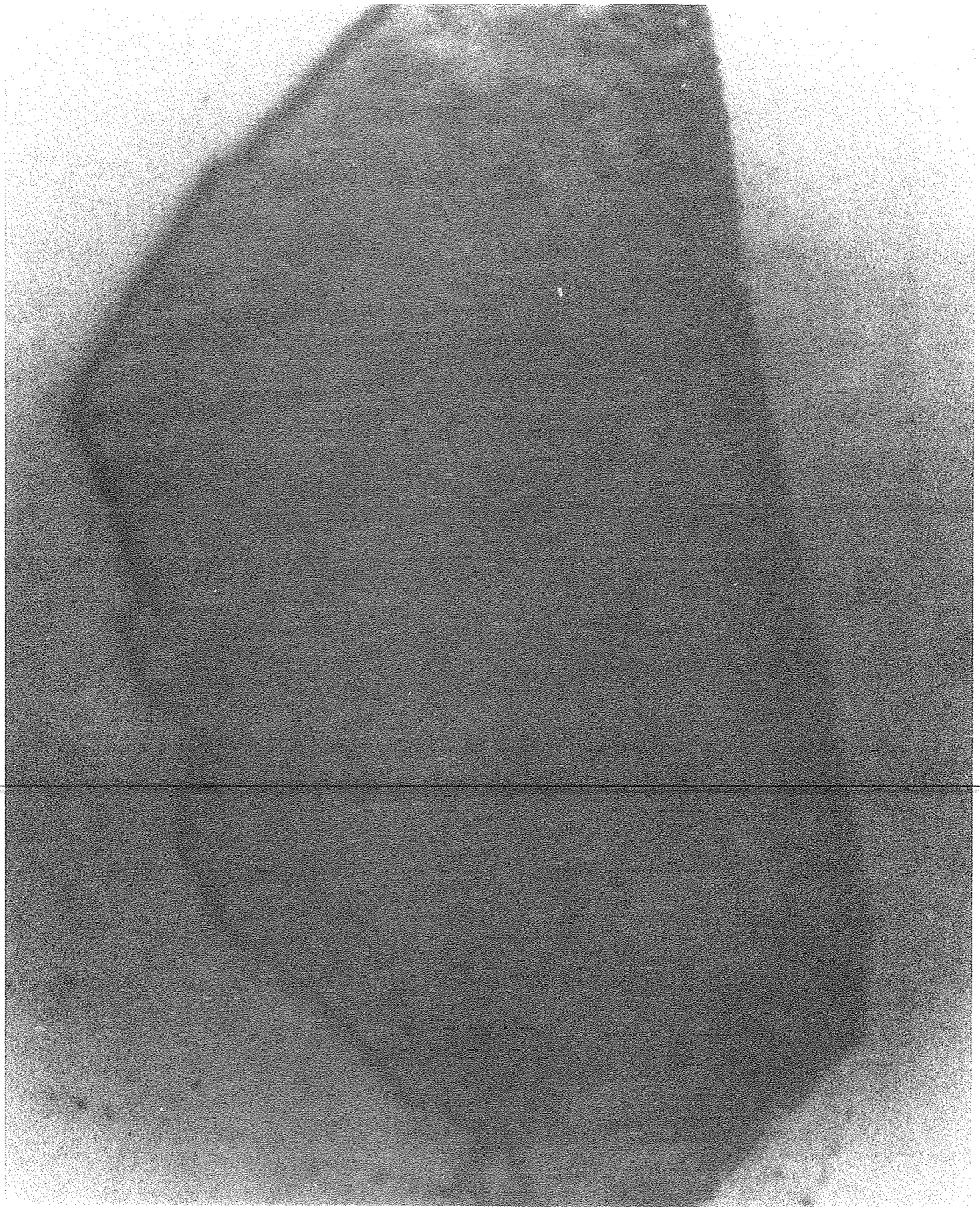

Figure 7a

XBB 785-5983

b

XBB 785-5982

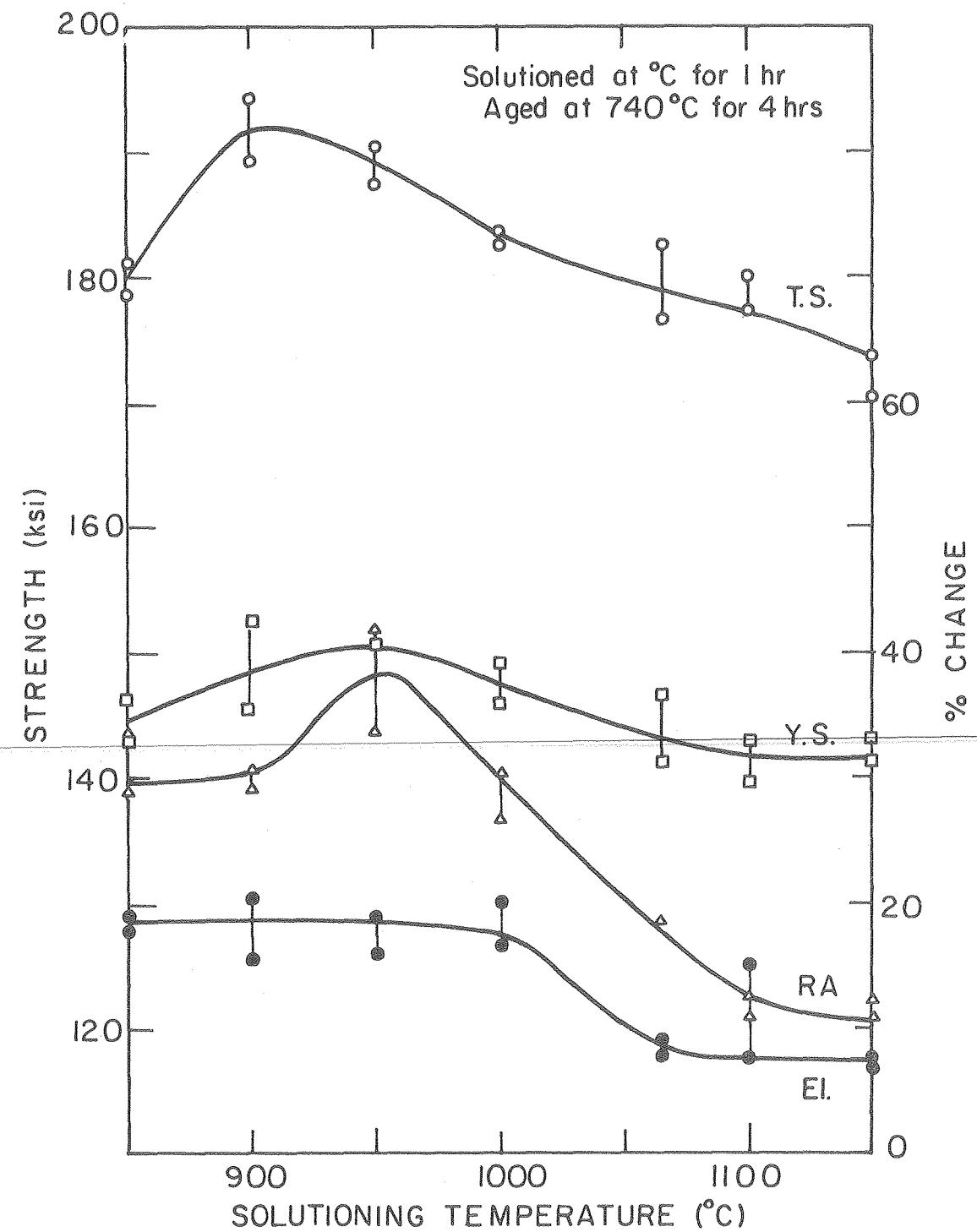

Figure 8 XBL 785-5006

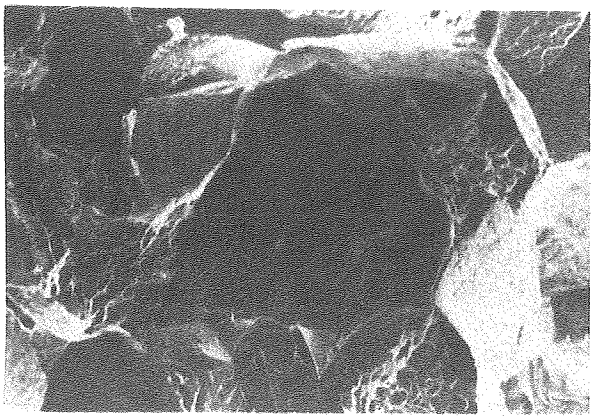

a

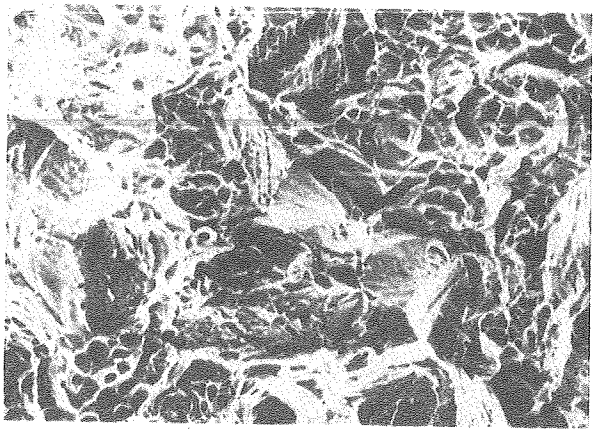

b

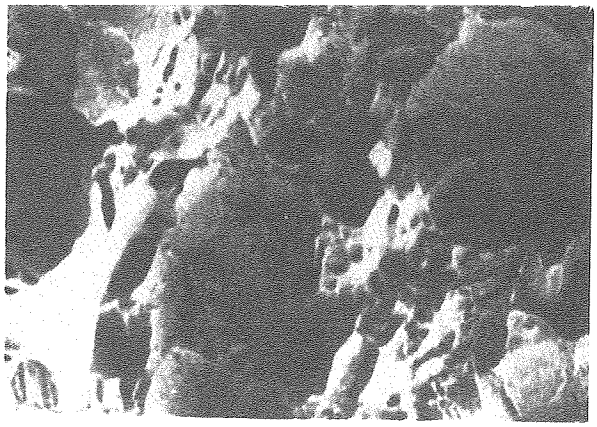

c XBB 785-5988

Figure 9

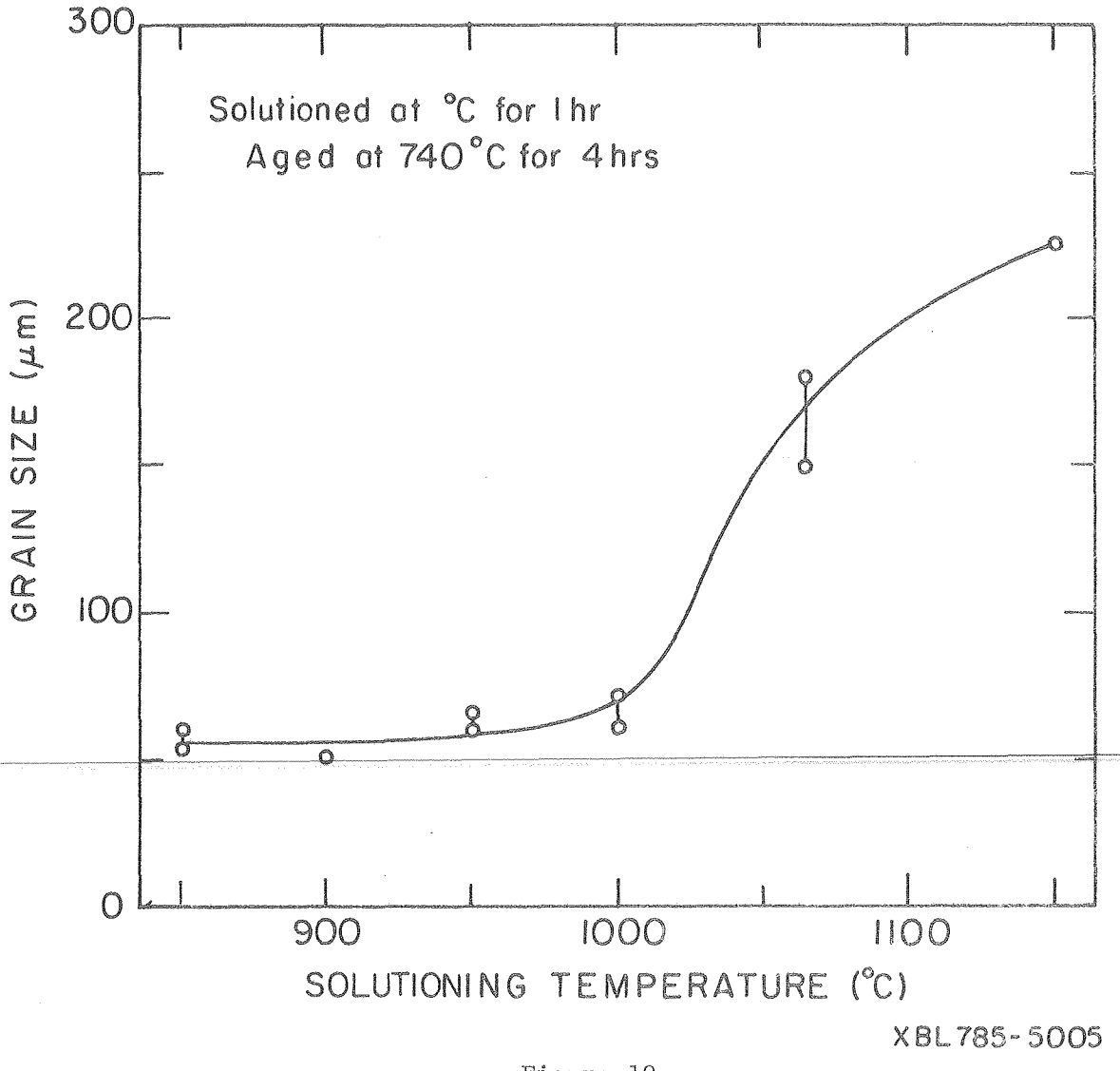
300
200
100
0
Solutioned at °C for 1 hr
Aged at 740°C for 4 hrs
GRAIN SIZE (μm)
900
1000
1100
SOLUTIONING TEMPERATURE (°C)
XBL785-5005

Figure 10

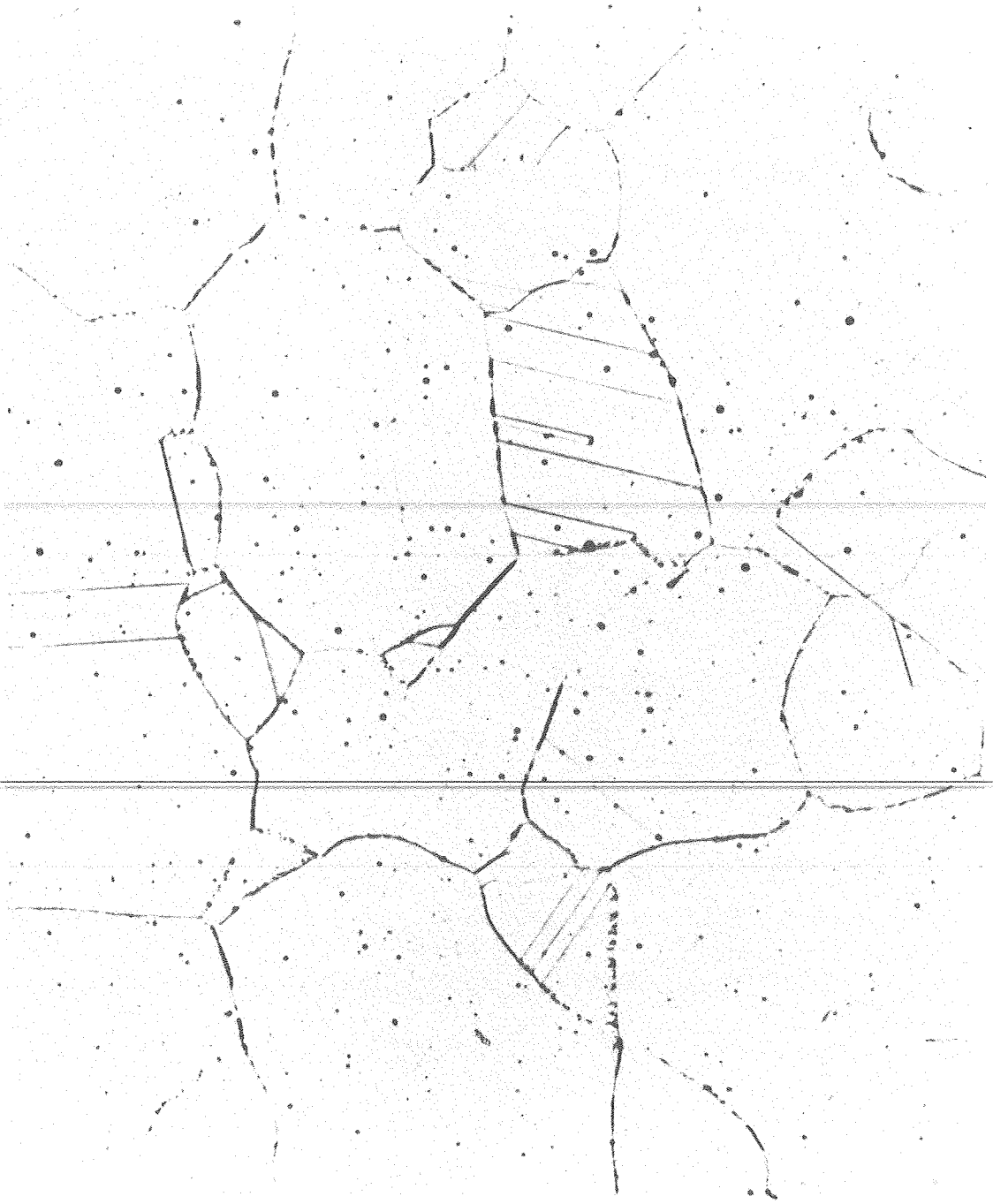

Figure 11a

XBB 785-5984

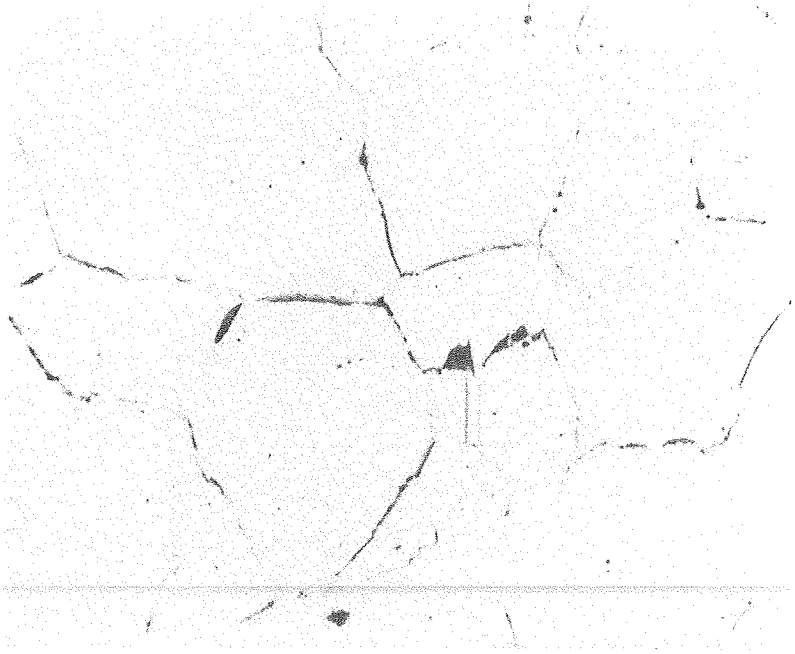

b

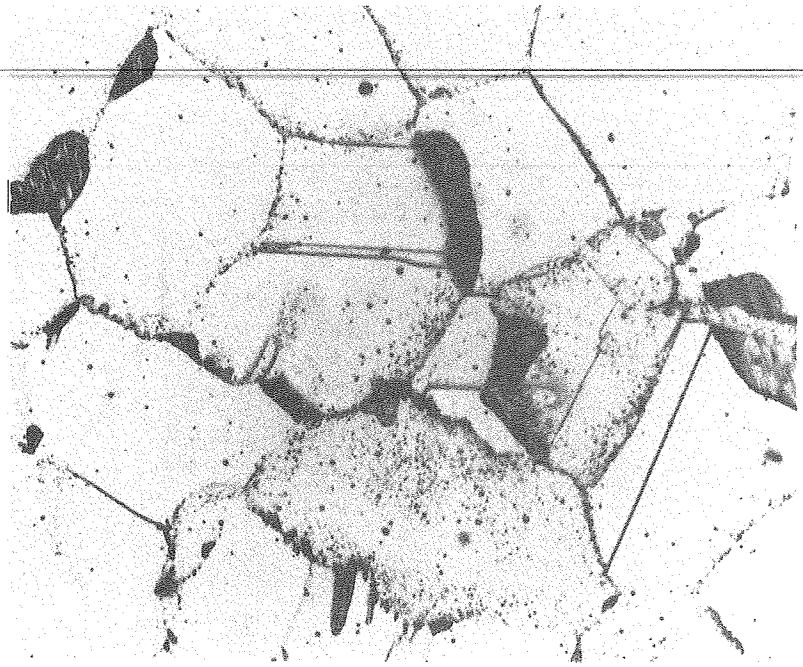

c

XBB 785-5990

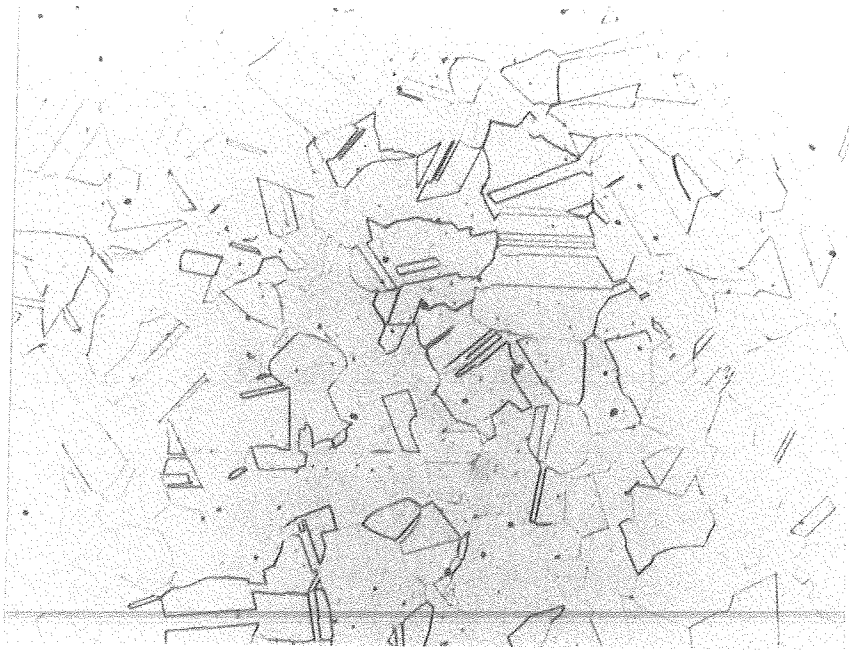

a

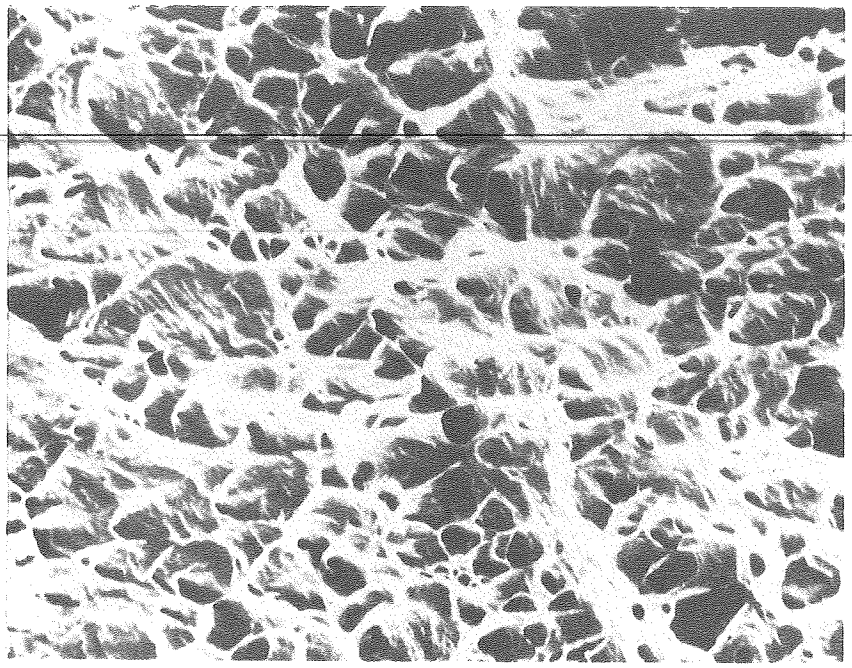

b

Figure 12 XBB 785-5986

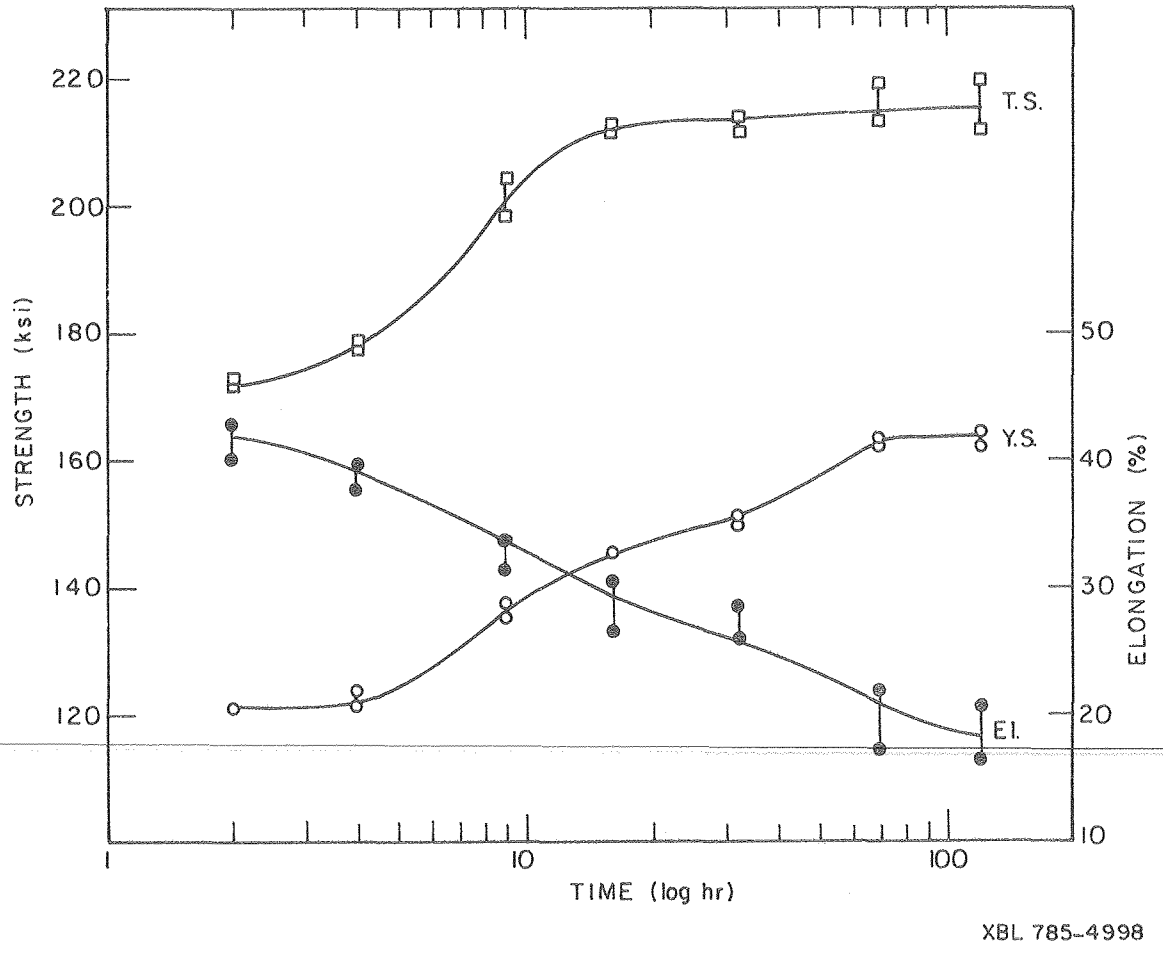
220
200
180
160
140
120
STRENGTH (ksi)
T.S.
Y.S.
El.
50
40
30
20
10
ELONGATION (%)
1
10
100
TIME (log hr)
XBL 785-4998

Figure 13

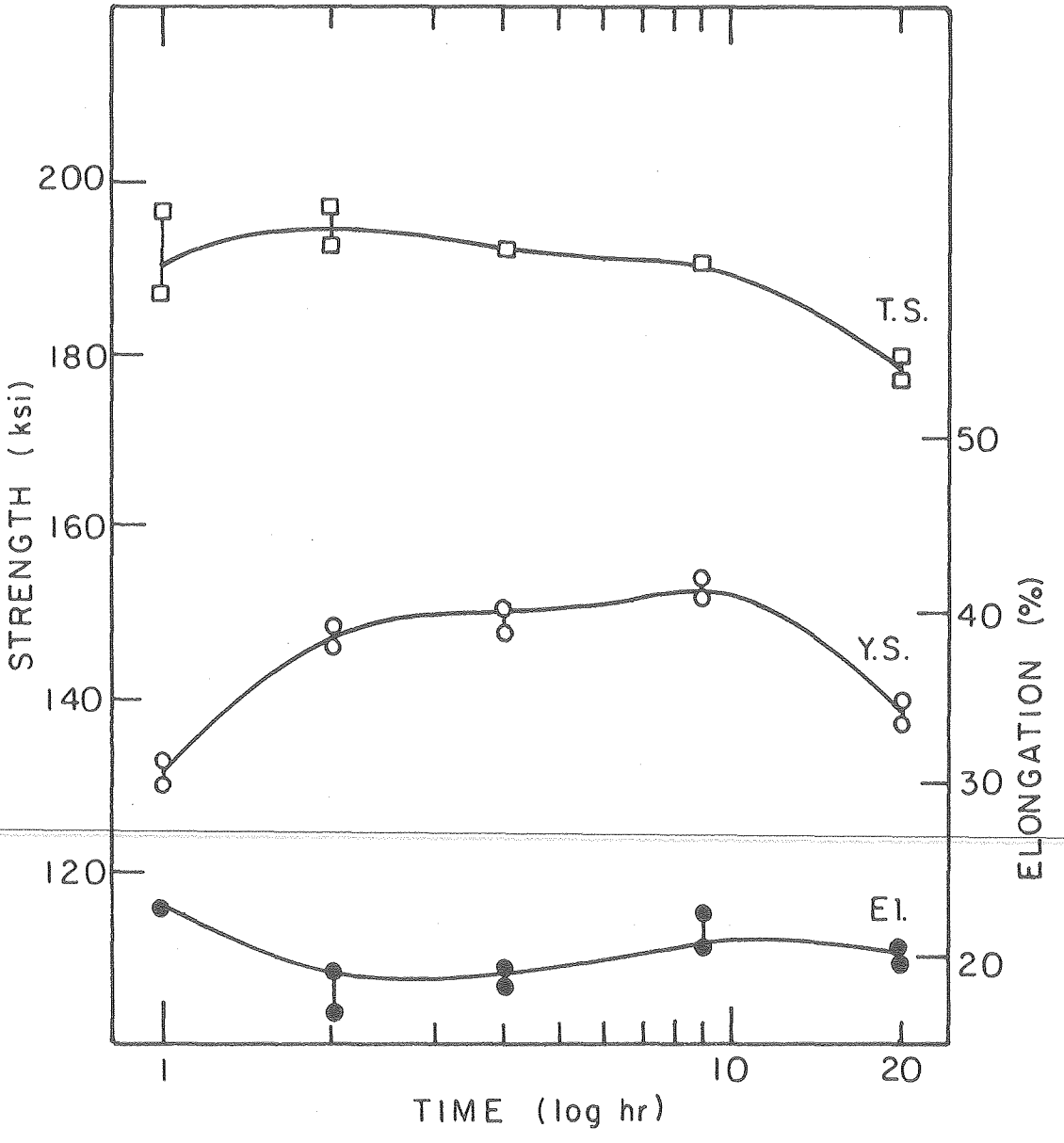
200
180
160
140
120
STRENGTH (ksi)
T.S.
Y.S.
El.
50
40
30
20
ELONGATION (%)
1
10
20
TIME (log hr)
XBL 785 - 4997

Figure 14

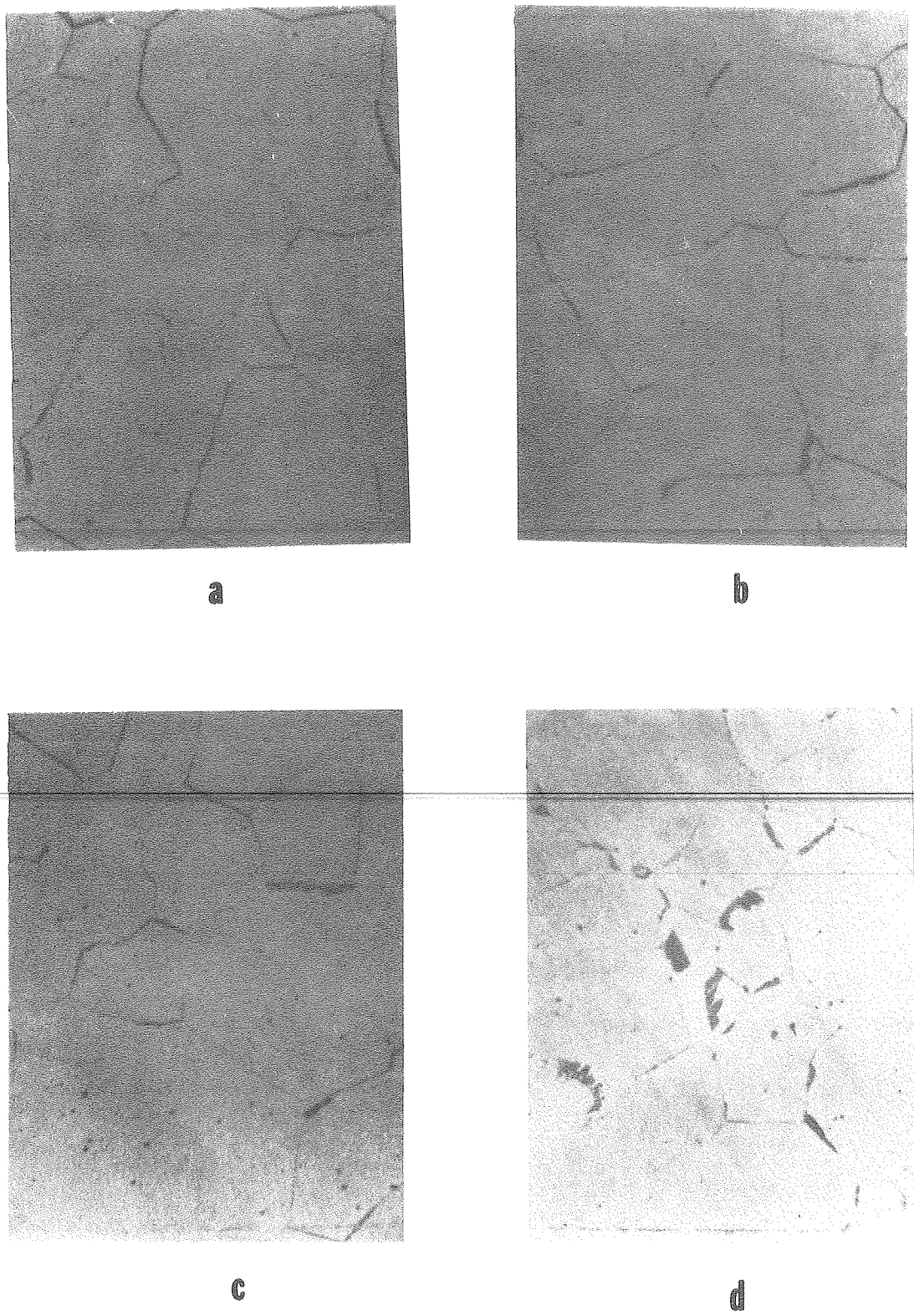

Figure 15 XBB 785-5994

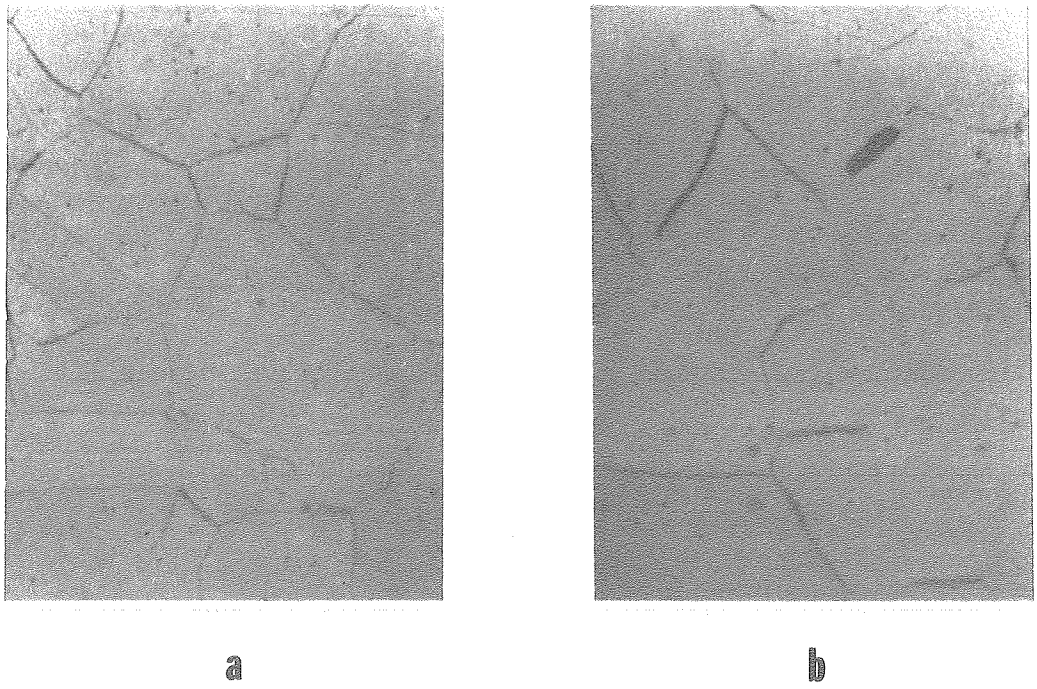

a b

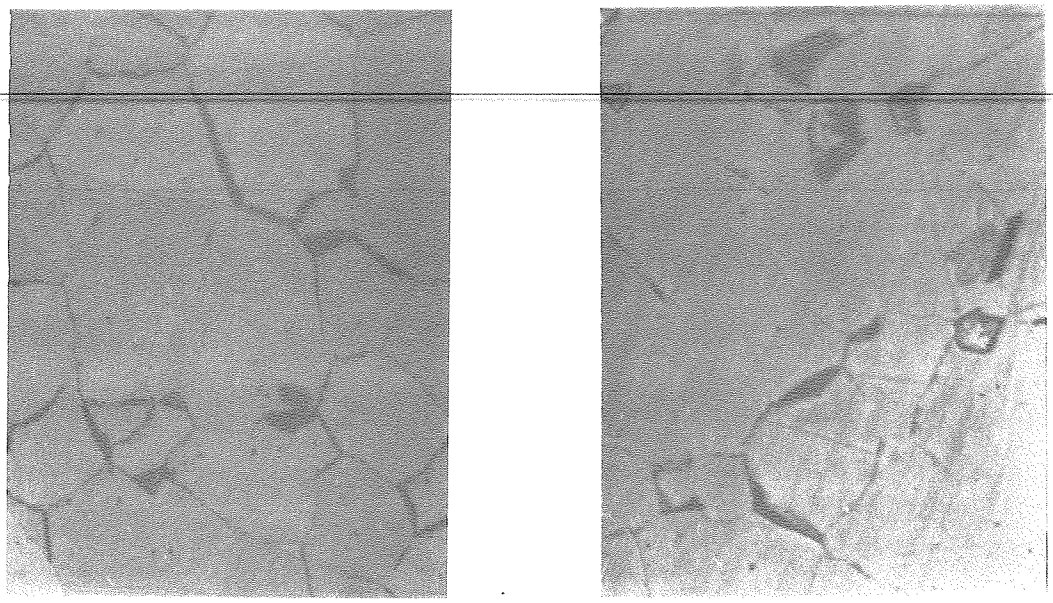

c d

Figure 16 XBB 785-5993

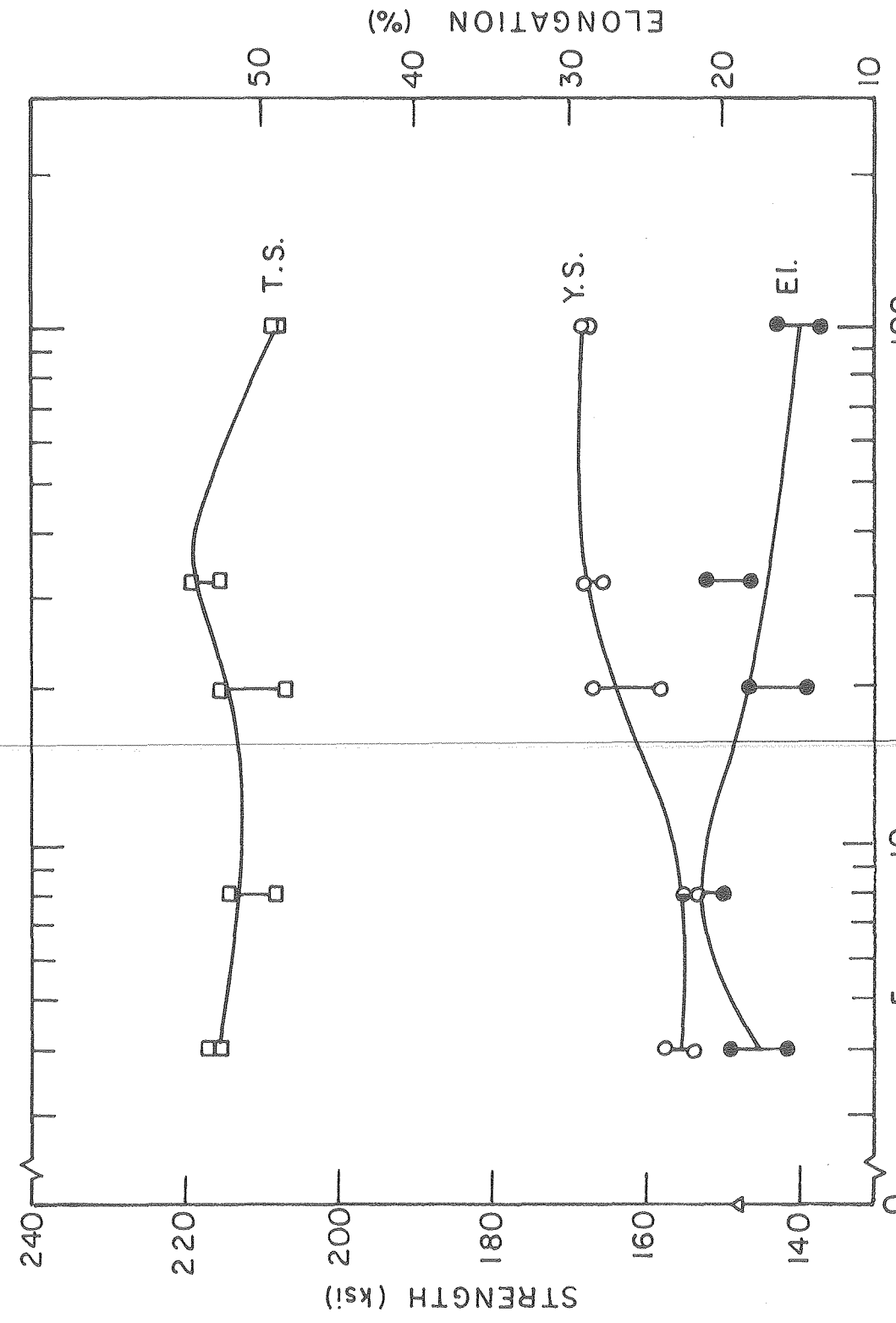

XBL785-4996

Figure 17

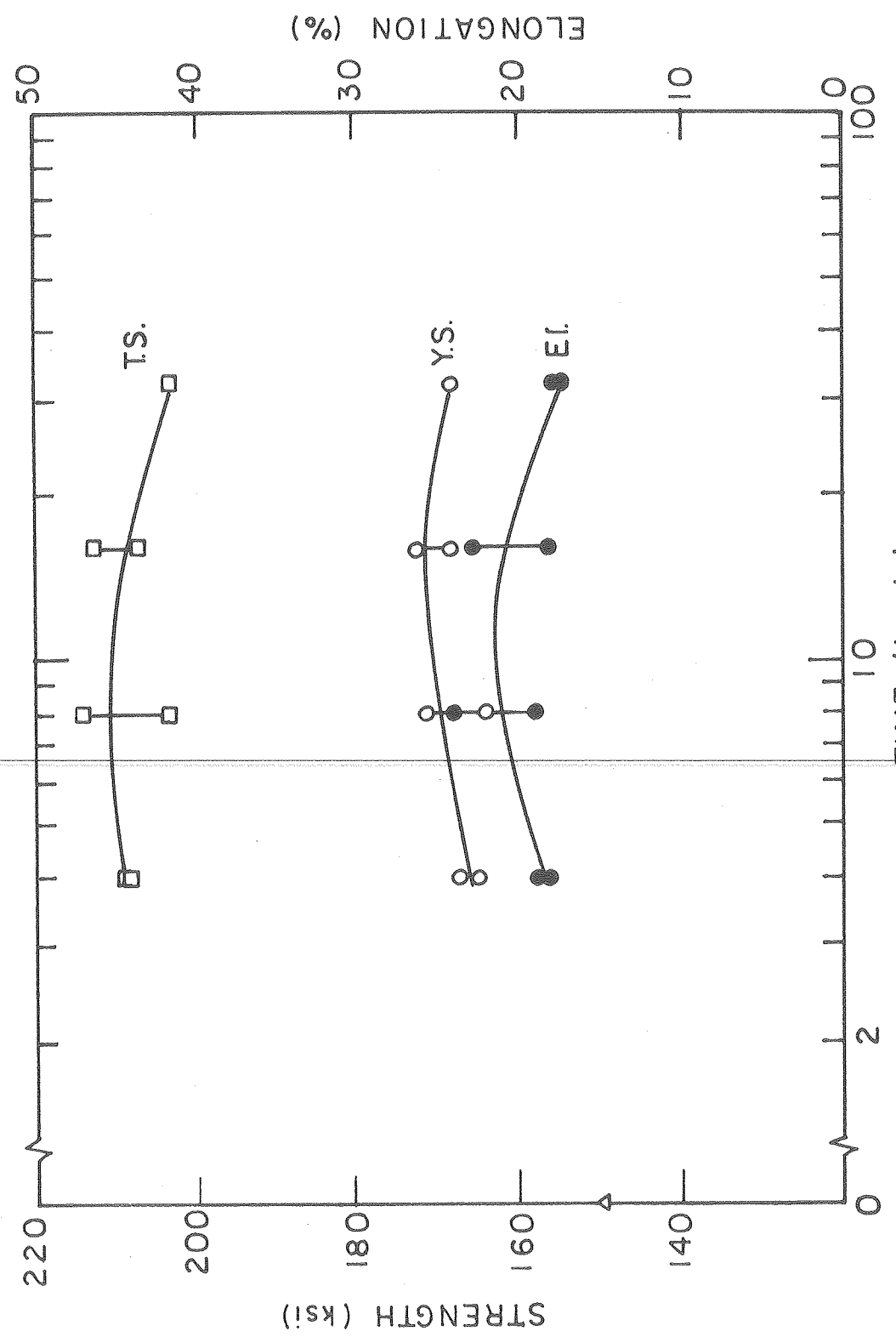

XBL 785-4995

Figure 18

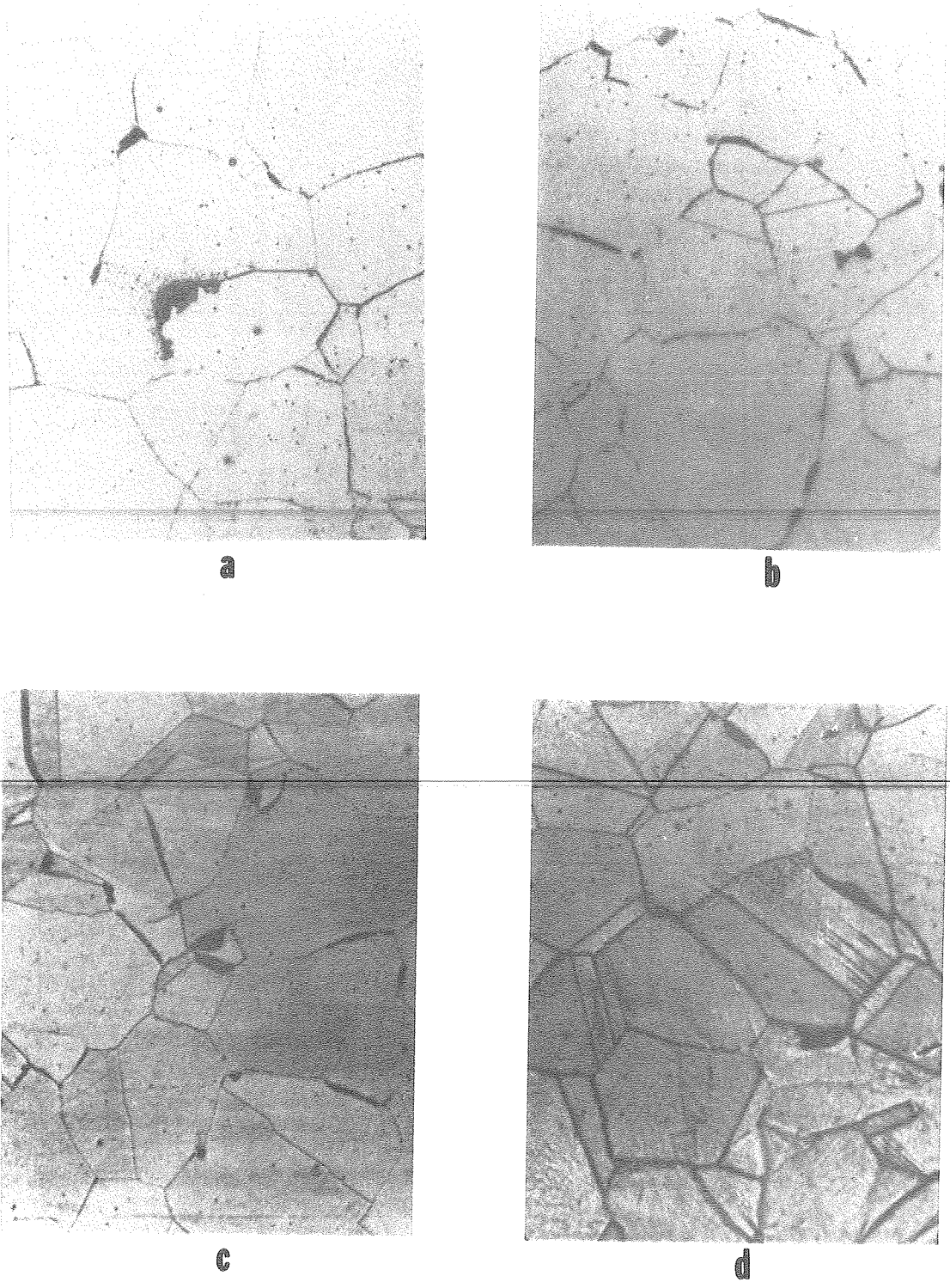

Figure 19

XBB 785-5985

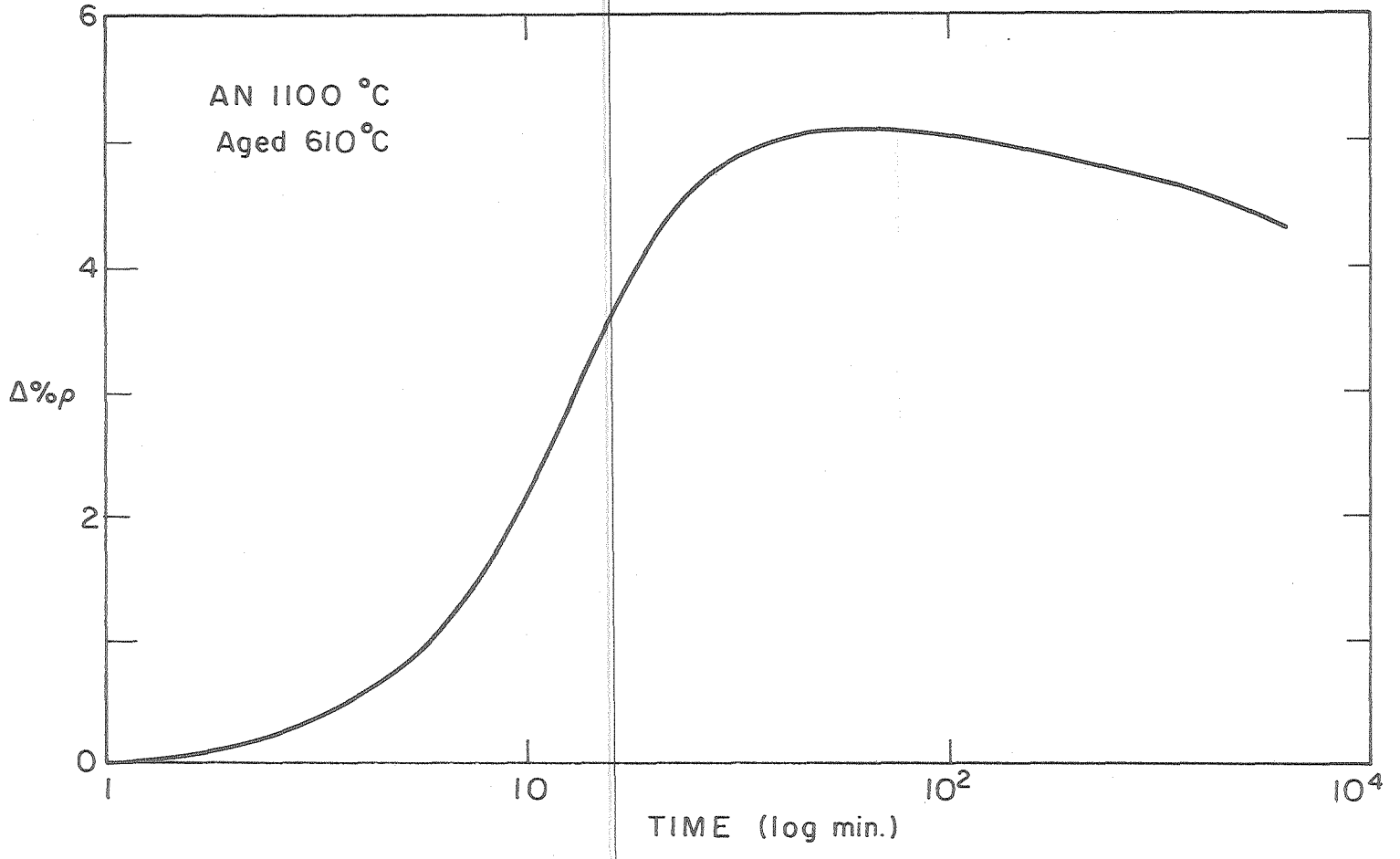

Figure 20

XBL785-4990

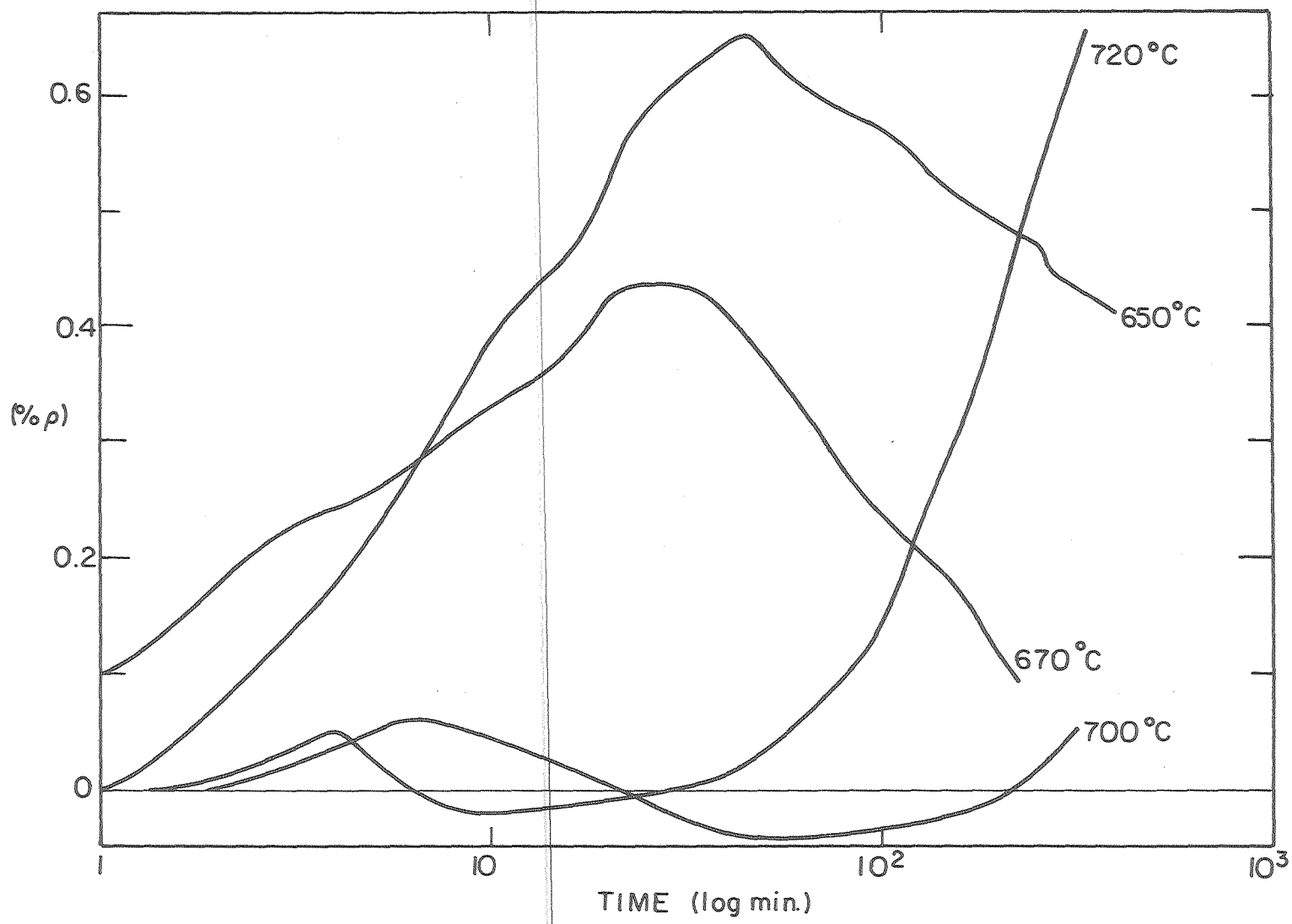

Figure 21

XBL785-4991

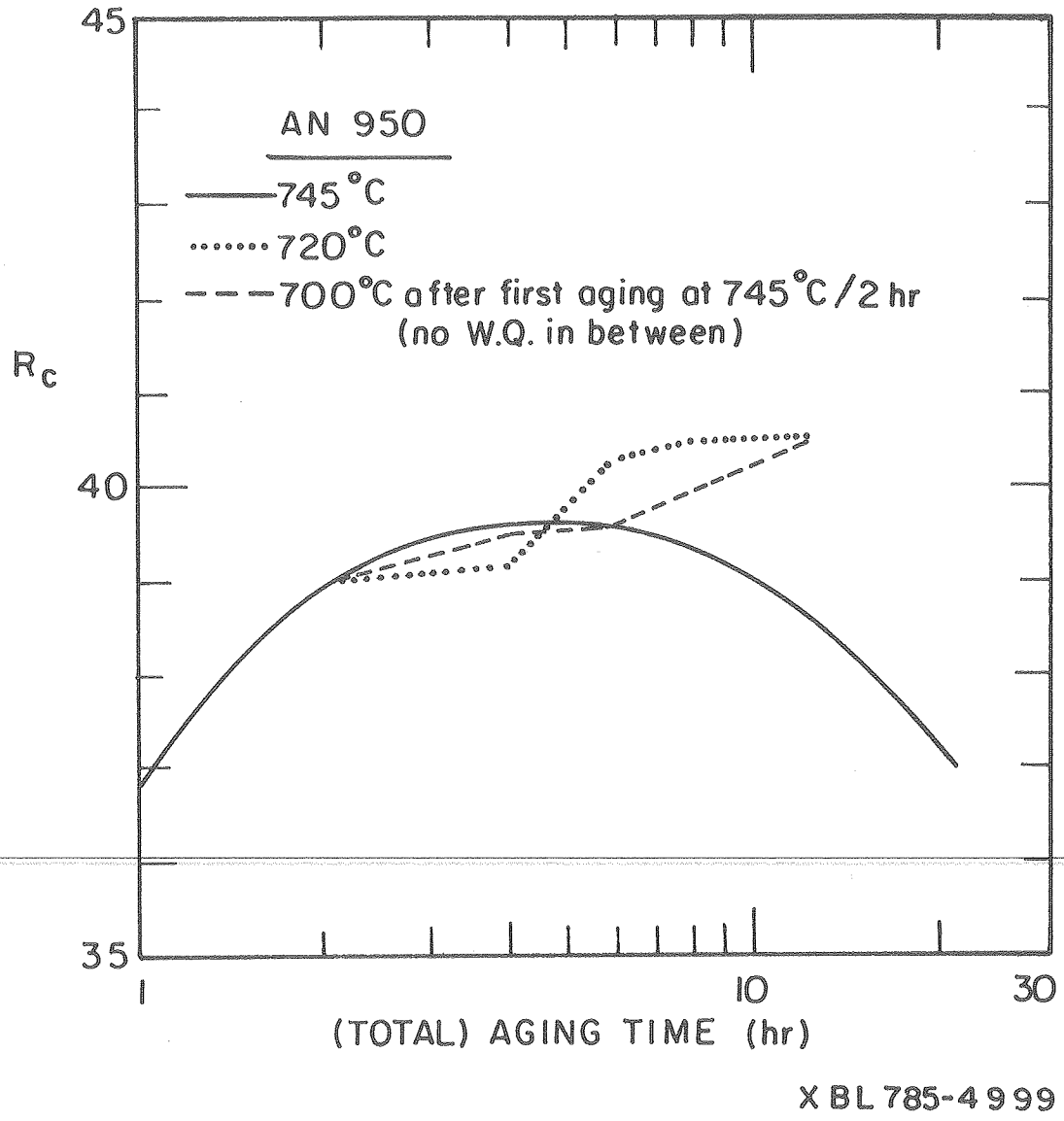
45
40
35
AN 950
745°C
720°C
700°C after first aging at 745°C/2 hr
(no W.Q. in between)
R_c
1
10
30
(TOTAL) AGING TIME (hr)
XBL785-4999

Figure 22

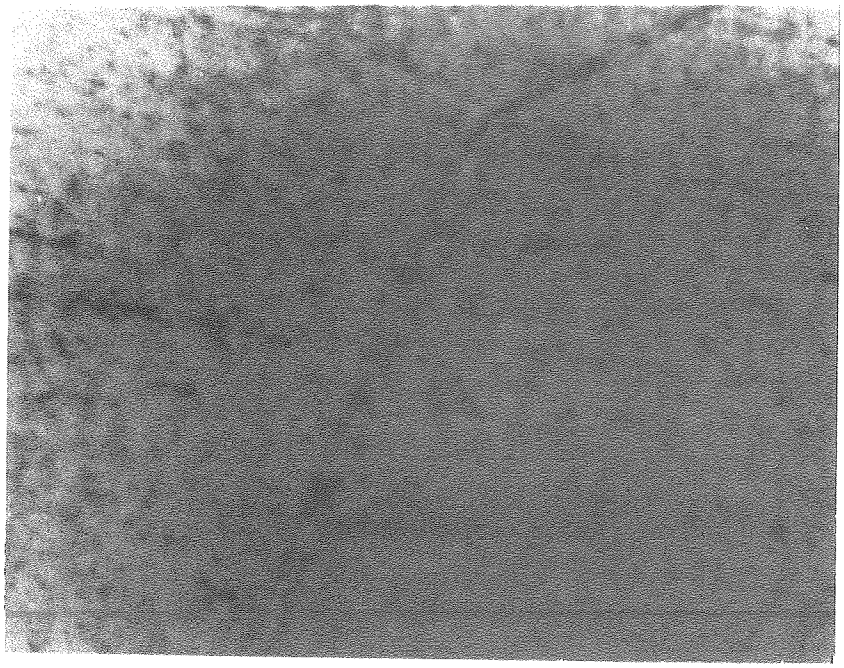

a

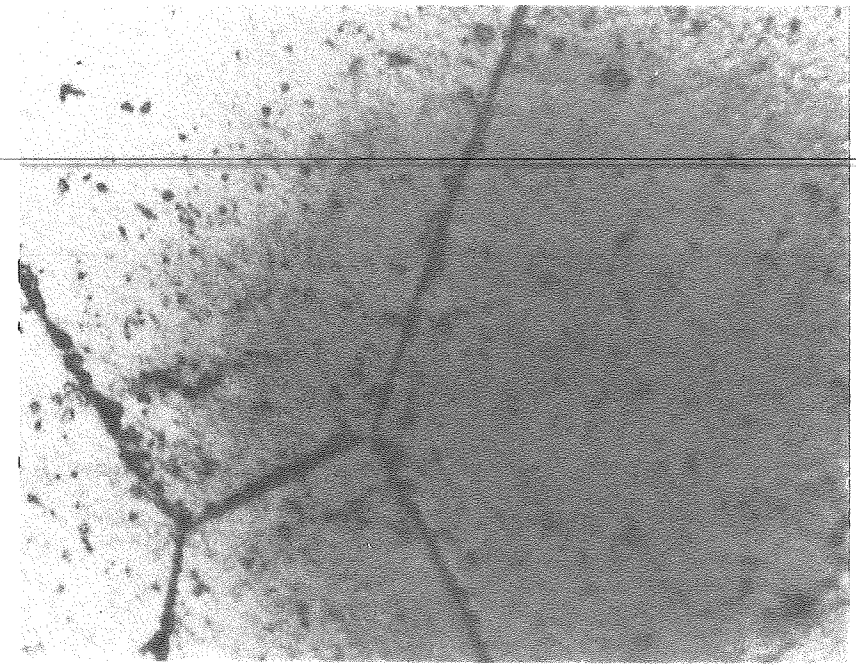

b

Figure 23 XBB 785-5987

This report was done with support from the Department of Energy. Any conclusions or opinions expressed in this report represent solely those of the author(s) and not necessarily those of The Regents of the University of California, the Lawrence Berkeley Laboratory or the Department of Energy.

TECHNICAL INFORMATION DEPARTMENT
LAWRENCE BERKELEY LABORATORY
UNIVERSITY OF CALIFORNIA
BERKELEY, CALIFORNIA 94720